공학석사학위논문

Aero-optical characteristics induced by shock wave in hypersonic flow field

극초음속 유동 내 충격파에 의한 공기광학 특성

2015 년 2 월

서울대학교 대학원

기계항공공학부

이 상 윤

Aero-optical characteristics induced by shock wave in hypersonic flow field

극초음속 유동 내 충격파에 의한 공기광학 특성

지도교수 정 인 석

이 논문을 공학석사 학위논문으로 제출함

2015 년 2 월

서울대학교 대학원

기계항공공학부

이 상 윤

이상윤의 공학석사 학위논문을 인준함

2015 년 2 월

위 원 장 _____ (인)

부위원장 _____ (인)

위 원 _____ (인)

Abstract

Aero-optical characteristics induced by shock wave in hypersonic flow field

Lee Sang-yoon
Department of Aerospace Engineering
The Graduate School
Seoul National University

Hypersonic flow field around flight vehicle is complicated and induce various problem. Especially, flight vehicle with optical system experience aero-optical aberration induced by hypersonic flow field. Aero-optics is a field which studies interaction between flow field and electromagnetic wave propagation near flight vehicle. Turbulence, shock wave and boundary layer at near flow field of flight vehicle induce index of refraction variation, distorting electromagnetic wave propagation characteristics. Aero-optical phenomena decrease optical performance and limits accuracy of optical system loaded on flight vehicle. Research have been conducted to find out the relation between flow field characteristics and optical characteristics. Accordingly, various devices have been developed to measure and analyze aero-optical characteristics. Recently, a device called Shack-Hartmann sensor was developed and compared with previous devices.

In this thesis, hypersonic flow field is demonstrated through shock tunnel and aero-optics experiment is conducted. Shock tunnel performance is validated by analyzing pressure distribution inside driven tube and measuring test time inside test section. Conical nozzle and contoured nozzle is installed at the shock tunnel to generate Mach 7 flow. Nozzle flow characteristics is studied through stagnation

pressure measurement with pitot rake and flow visualization with shadowgraph or schlieren method. Conical nozzle has 63% decrease of stagnation pressure and exit flow has Mach 6.8. Contoured nozzle has little loss of stagnation pressure and exit flow is Mach 6.9.

After shock tunnel performance and nozzle performance is validated, aero-optical characteristics is measured using Shack-Hartmann sensor. Shack-Hartmann sensor performance is studied and validated with experiments on optical table. Wedged window and hot wire is used as a density disturbance. Wedged window tilts the laser to angle which is same as refractive angle calculated through refraction law. Hot wire experiment result reveals increase of optical aberration as power consumption of hot wire increase. Aero-optical characteristics induced by shock wave in hypersonic flow field is studied. Wedged model is installed inside shock tunnel test section and Shack-Hartmann sensor measured phase and intensity, which is converted to point spread function (PSF). From PSF, aero-optical parameter such as bore sight error (BSE), Strehl ratio is calculated. In the results, average BSE and tilt increased as stagnation pressure increased. Average BSE is 80 ~ 160 μ rad, and Strehl ratio is 0.65 ~ 0.835. Shock wave in hypersonic flow increase BSE, tilt and decrease Strehl ratio.

Keywords : Hypersonic flow, Shock tunnel, Aero-optics
Shack-Hartmann sensor

Student Number : 2013-20694

Table of Contents

List of Tables

List of Figures

Nomenclature

Alphabet

B: Point spread function peak intensity displacement on CCD

B_m: Equivalent magnified length of B before beam reducer

D_{input}: Incidence beam diameter of beam reducer

D_{output}: Output beam diameter of beam reducer

f_1: focal length of lens1 in beam reducer

f_2: focal length of lens2 in beam reducer

f_{La}: Focal length of Shack-Hartmann sensor lens array

L: Distance between model window and Shack-Hartmann sensor CCD

M: Mach number

M_a: Mach number before shock wave

M_b: Mach number after shock wave

M_r: Mach number of reflected shock wave in shock tube theory

p_1, p_2, p_3, p_4: Pressure at each state in shock tube

p_a: Static pressure before shock wave

p_b: Static pressure after shock wave

p_0: Stagnation pressure

p_{0a}: Stagnation pressure before shock wave

p_{0b}: Stagnation pressure after shock wave

T_1, T_2, T_3, T_4: Temperature at each state in shock tube

T_a: Static temperature before shock wave

T_b: Static temperature after shock wave

u_s: Shock speed

Greek

α_s: Bore sight error obtained from Shack-Hartmann sensor

α_c: Calculated bore sight error based on model window

γ_1, γ_2, γ_3, γ_4: Ratio of specific heats at each state in shock tube

γ: Ratio of specific heats (assumed as 1.4 throughout the thesis)

θ; Wedge angle of wedge model

1. Introduction

1.1 Background

Various objects entering atmosphere, such as satellite or flight vehicles, have potential of impacting the ground and cause serious damage. Thus atmosphere should be monitored and occasionally bring objects down by flight vehicles departed from ground. As object approach the ground, speed usually increase up to hypersonic. Therefore Flight vehicle tracing the object also has to be hypersonic to follow up before the object arrive on ground. However in hypersonic flight, flow around the vehicle is complicated inducing various problems. One important issue is distortion of image acquired by guidance seeker. Flight vehicle usually traces the object by sensing the electromagnetic wave transmitted from the object through sensor on the flight vehicle. Electromagnetic wave propagation is effected by flow around the vehicle and tracing of the flight vehicle degrades. In this thesis, hypersonic flow field and its effect on optical propagation is studied.

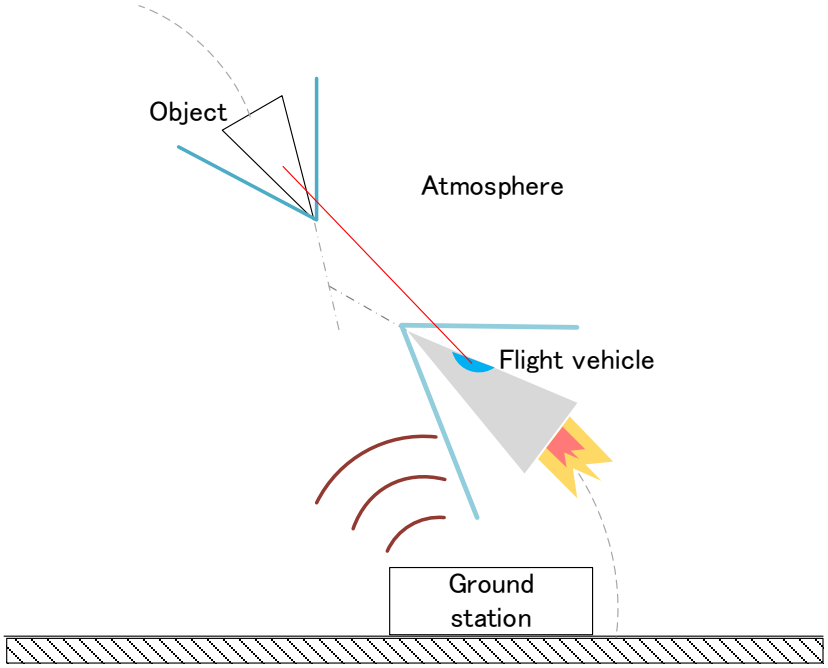

Figure 1.1 Schematic diagram of object interception.

1.2 Hypersonic flow field around flight vehicle

In hypersonic flight, flow around the vehicle is complicated due to shock waves, boundary layer, turbulence etc. Especially shock wave is inevitable in flow over sonic speed. As speed increase, shock wave strength increase and impact on hypersonic flow property also increase. Shock wave is usually predictable through theory, but flow components such as turbulence, boundary layer etc. is difficult to predict. Especially interaction between flow components is difficult to predict. Therefore experiment is necessary to study hypersonic flow field characteristics. Generally wind tunnel is used to demonstrate flow field on ground and study flow field characteristics around flight vehicle. For hypersonic flow demonstration, high enthalpy wind tunnel, such as shock tunnel, is used.

1.3 Aero-Optics

One way of guiding a flight vehicle to an object is installing sensor on the flight vehicle. Sensor acquires image of the object by capturing the electromagnetic wave from the object, and recognizes the position of the object to follow it. During propagation of the electromagnetic wave from the object toward flight vehicle, flow disturbance such as shock wave, turbulence, boundary layer etc. induce density fluctuation. Since density has linear relation with refractive index, electromagnetic wave propagating through flow disturbance is distorted.

Depending on electromagnetic wave propagation region, fields studying interaction between flow field and optical characteristics can be categorized to two. First field of study is “atmospheric propagation”. Atmospheric propagation studies interaction of optical characteristic and flow disturbance during propagation through atmosphere. Effect of flow disturbance such as atmospheric turbulence is studied. Second field of study is aero-optics. Aero-optics study interaction of flow disturbance and optical characteristics during propagation near flow field of flight

vehicle. Usually turbulence, shock wave, boundary later induced optical aberration is studied. Current thesis focuses on optical aberration induced by aero-optical phenomena.

Figure 1.2 is schematic diagram of aero-optical phenomena occurred at flight vehicle. Sensor on the flight vehicle captures distorted signal and recognizes the target as located on different place. This sort of aberration is called Bore Sight Error (BSE). Since propagation direction changes, phase of the electromagnetic wave includes tilt. Intensity of electromagnetic wave also changes, usually reduced. Strehl ratio represents the decrease in electromagnetic wave intensity. Strehl ratio is usually a criterion of optical degradation. Throughout this thesis, aero-optics parameter such as BSE, tilt, Strehl ratio is studied.

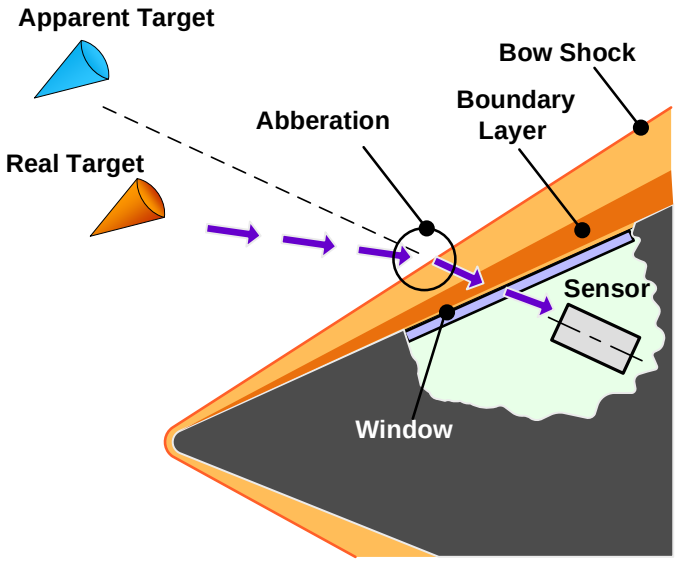

Figure 1.2 Aero-optical phenomena occurred at flight vehicle.

1.4 Previous Study

Aero-optics has been studied since Liepmann, who made an attempt to quantify aero-optical aberration in 1950s [1]. Since then, various efforts were made to relate

optical characteristics with flow characteristics and to measure aero-optical aberration. Recently, Shack-Hartmann sensor, which is a device that acquires phase and intensity, is developed and used in research. In this thesis, two research will be introduced. First research measured aero-optical aberration in hypersonic flow field using Shack-Hartmann sensor. Second research conducted aero-optics experiment in hypersonic flow field using other optical sensors.

Research team in Arnold Engineering Development Center (AEDC) conducted aero-optics experiment in shock tunnel (Tunnel 9) [2]. In this research, free stream condition at test section was Mach 7, p_0 17.7 – 80.5 Mpa, T_0 1932 K. Three devices were used to measure optical aberration induced by flow field around 15˚ angle wedge. Imaging camera system (ICS) and X-Y detector were used to measure far field pattern directly and Shack-Hartmann sensor was used to measure near field pattern. Point spread function (PSF) was acquired from Shack-Hartmann sensor measured phase and intensity. Far-field pattern from ICS and PSF from Shack-Hartmann sensor were compared and both showed similar result. From this research Shack-Hartmann sensor performance was validated to use in aero-optics experiment.

Research team in Calspan-University at Buffalo Research Center (CUBRC) conducted aero-optics experiment in Large Energy National Shock Tunnel (LENS) facility [2, 3]. Nozzle exit flow condition was Mach 9 - 11, stagnation pressure 120 - 150 Mpa, stagnation temperature 600 - 6200 K. Holography, point source imagery, radiometry, spectrometry were used to measure aero-optical characteristics. With these instruments, bore sight shifting, intensity reduction (Strehl ratio) were acquired. 2-D wedge model and 3-D cone model were used for experiment. 2-D wedge model and 3-D cone model showed similar results. Parameters that quantify aero-optical aberration and model design was referenced from this research.

1.5 Research objectives

Demonstrate hypersonic flow on ground

Hypersonic flow demonstration is important on hypersonic flow experiment. This

thesis aims to demonstrate hypersonic flow with shock tunnel to study flow characteristics. Shock tunnel operation principle is studied and performance is validated. Hypersonic flow at the nozzle exit is studied using wedge model and pitot rake. Pressure sensor and visualization technique are used to study hypersonic flow field.

Establish aero-optics experiment method in shock tunnel application

Aero-optics experiment is necessary to study effect of aero-optics on optical system performance. In aero-optics experiment, beam propagation characteristics is measured with optical sensor. Simultaneously with optical measurement, flow field measurement should be conducted to study the effect on optical characteristics. Since measurement is quite complicated experiment method should be considered. This thesis aims to establish aero-optics experiment method. Aero-optical parameters are investigated and optical measurement method using Shack-Hartmann sensor is studied. To understand principle of Shack-Hartmann sensor and to establish aero-optical parameter acquisition process from the sensor, static flow experiment is conducted on the optical table. Known density disturbance, such as window, is used and aberration on light source is verified. Designing optical components such as beam guiding or beam size modifying is also studied.

Observe effect of shock wave on aero-optical aberration

Flight vehicle in supersonic flow generally contains shock wave. Shock wave induce considerable density difference, comparing to other flow phenomena. Thus it is expected that shock wave affects aero-optical aberration relatively significant comparing to other flow phenomena. This thesis also aims to study Aero-optical characteristics induced by shock wave in hypersonic flow field. 10˚ Wedge model is designed and installed in Mach 7 shock tunnel test section to conduct aero-optics experiment. Effect of shock wave on aero-optical parameters such as BSE, tilt and Strehl ratio is studied.

2. Experimental setup

2.1 Facility

Wind tunnel is a facility that demonstrates flight condition on ground. For hypersonic application, usually high stagnation enthalpy is necessary. Various method is used to increase stagnation enthalpy of test flow in hypersonic wind tunnel. Shock tunnel is one type of wind tunnel that achieves high enthalpy with moving shock wave.

Main component of shock tunnel is shock tube, nozzle and test section. Shock tube consist of driver tube and driven tube. Figure 2.1 shows typical wave propagation inside a shock tube of the shock tunnel. When high pressure gas (state 4) and low pressure gas (state 1) contacts suddenly inside a shock tube, moving shock wave is produced and propagates through low pressure gas region. At the other end of the driven tube, shock wave reflects and produces state 5 region at the diagram. State 5 region has high pressure and high temperature region with no velocity. Therefore state 5 region becomes stagnation region of the nozzle flow. Conditions in state 5 is calculated as following procedure [4]:

(Derive p2/p1) $\frac{\boldsymbol{p_4}}{\boldsymbol{p_1}} = \frac{\boldsymbol{p_2}}{\boldsymbol{p_1}}\left[1 - \frac{(\gamma_4-1)\left(\frac{a_1}{a_4}\right)\left(\frac{\boldsymbol{p_2}}{\boldsymbol{p_1}}-1\right)}{\sqrt{2\gamma_1\left[2\gamma_1+(\gamma_1+1)\left(\frac{\boldsymbol{p_2}}{\boldsymbol{p_1}}-1\right)\right]}}\right]^{-\frac{2\gamma_4}{\gamma_4-1}}$, (2.1)

(Derive shock speed u_s) $u_s = a_1 M_s = \sqrt{\gamma_1 R_1 T_1}\left[\left(\frac{\boldsymbol{\gamma_1+1}}{\boldsymbol{2\gamma_1}}\frac{\boldsymbol{p_2}}{\boldsymbol{p_1}} + \frac{\boldsymbol{\gamma_1-1}}{\boldsymbol{2\gamma_1}}\right)\right]$, (2.2)

(Derive reflected shock speed M_r) $\frac{M_r}{M_r^2-1} = \frac{M_s}{M_s^2-1}\sqrt{1 + \frac{2(\boldsymbol{\gamma_1-1})}{(\boldsymbol{\gamma_1+1})^2}(M_s^2-1)\left(\gamma_1 + \frac{1}{M_s^2}\right)}$, (2.3)

(Derive pressure p_5/p_2) $\frac{p_5}{p_2} = 1 + \frac{2\boldsymbol{\gamma_2}}{\boldsymbol{\gamma_2+1}}(M_r^2-1)$, (2.4)

(Derive pressure T_5/T_2) $\frac{T_5}{T_2} = \left[1 + \frac{2\boldsymbol{\gamma_2}}{\boldsymbol{\gamma_2+1}}(M_r^2-1)\right]\left[\frac{\frac{\boldsymbol{\gamma_1+1}}{\boldsymbol{\gamma_1-1}} + \left(\frac{p_5}{p_2}\right)}{1+\frac{\boldsymbol{\gamma_1+1}}{\boldsymbol{\gamma_1-1}}\left(\frac{p_5}{p_2}\right)}\right]$. (2.5)

Test is conducted while test region is sustained with no contamination of other waves inside the tube. Pressure of the gas inside the tube, type of driver and driven gas, temperature of the gas inside the tube is modified to produce test condition. Since temperature is almost at room temperature and type of gas is defined, various condition of test region is produced depending on the pressure of gas.

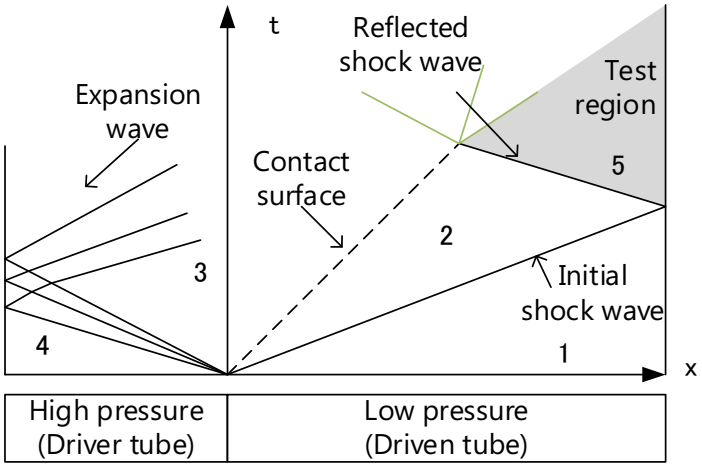

Figure 2.1 x-t diagram of shock tube.

AST-1 shock tunnel in Aerospace Propulsion and Combustion Laboratory (APCL) at Seoul National University (SNU) is used to demonstrate flight condition on ground. Figure 2.2 is the image of AST-1 shock tunnel. Nitrogen is used for driver gas and air is used for driven gas. PET film is used as the diaphragm for both end of the driven tube to contact gases suddenly. Thickness of PET film has linear relation with burst pressure. Maximum pressure that can be achieved with PET film is 13 Mpa. Two Types of nozzle are used to produce Mach 7 flow. One is conical nozzle and another is contoured nozzle. Size of Test section is 300x300x600 mm. Test section has window on each side and one window on top.

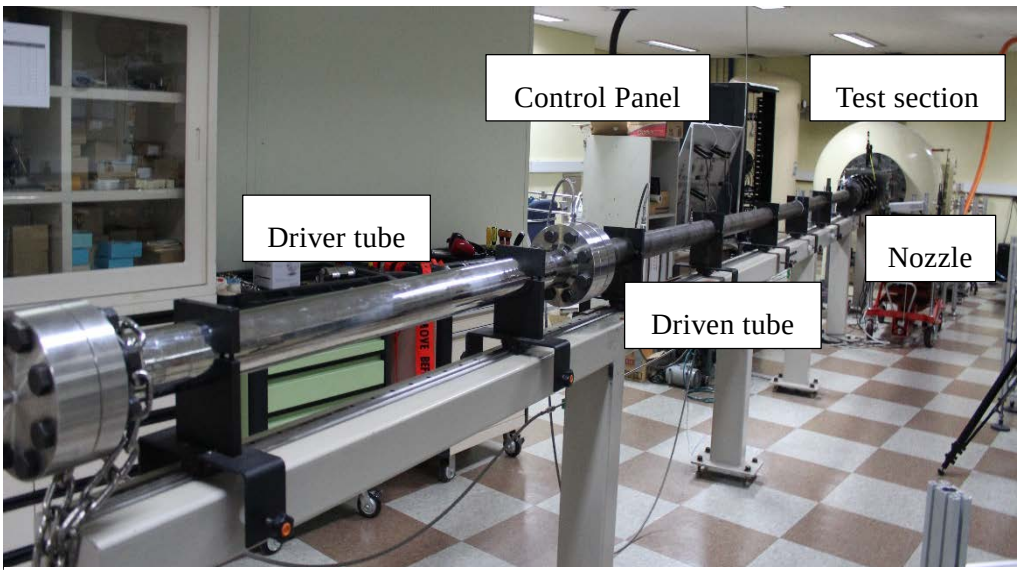

Figure 2.2 Image of AST-1 shock tunnel.

2.1.1 Conical nozzle

Conical nozzle is simple to design and manufacture. Typical conical nozzle schematic diagram is shown at figure 2.3. Conical nozzle is usually designed with constant expansion angle. Since flow just expands with constant angle, exit flow is not uniform and flow direction is not parallel with nozzle axis. Conical nozzle was designed by conducting viscous and inviscid numerical analysis[5]. Figure 2.4 is the image of conical nozzle installed at AST-1 shock tunnel. Conical nozzle expansion angle is 8.5˚, throat diameter is 12 mm, exit diameter is 150 mm and total length is about 500 mm.

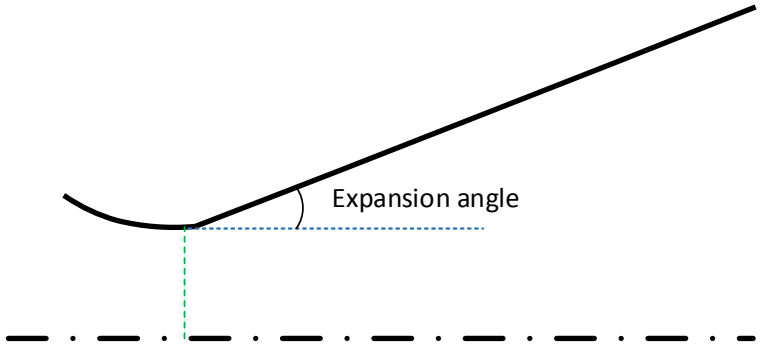

Figure 2.3 Schematic diagram of conical nozzle.

Figure 2.4 Conical nozzle installed at AST-1 shock tunnel.

2.1.2 Contoured nozzle

Figure 2.5 is schematic diagram of contoured nozzle. Surface of contoured nozzle has different inclination as it expands and cancels wave generated inside the contoured nozzle producing uniform exit flow. Usually contoured nozzle is designed through method of characteristics (MOC). Flow condition near throat, exit Mach etc. is defined and characteristics lines is drawn, starting from the throat. Inviscid contour is acquired from MOC. Since boundary layer at nozzle surface affects nozzle flow condition, inviscid contour was corrected[6]. Figure 2.6 is image of contoured nozzle

installed at AST-1 shock tunnel. Contoured nozzle throat diameter is 17.46 mm, exit diameter is 189 mm and total length is about 1100m. Since ratio of nozzle exit diameter 1.26 and ratio of throat diameter is 2.2, contoured nozzle has significantly longer length. Changing of inclination and long contour is a factor of difficulty in manufacturing process.

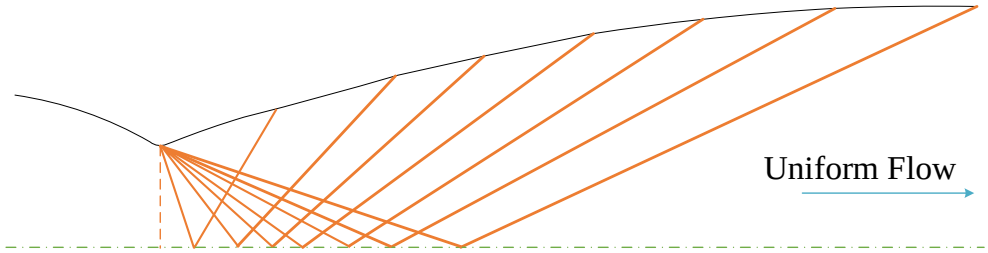

Figure 2.5 Schematic diagram of contoured nozzle.

Figure 2.6 Contoured nozzle installed at AST-1 shock tunnel.

2.2 Model design and installation

Aero-optics model is designed for experiment in shock tunnel. Figure 2.7 is schematic diagram of aero-optic model and figure 2.8 is image of aero-optics model installed in shock tunnel test section. Aero-optics model consist of 4 parts; laser, optical components, sensor and model. Laser beam becomes a plane wave through collimation lens, propagates through wedge model, guided with mirror, reduce the beam size appropriate for optical sensor aperture and finally optical sensor captures the beam to acquire optical aberration information.

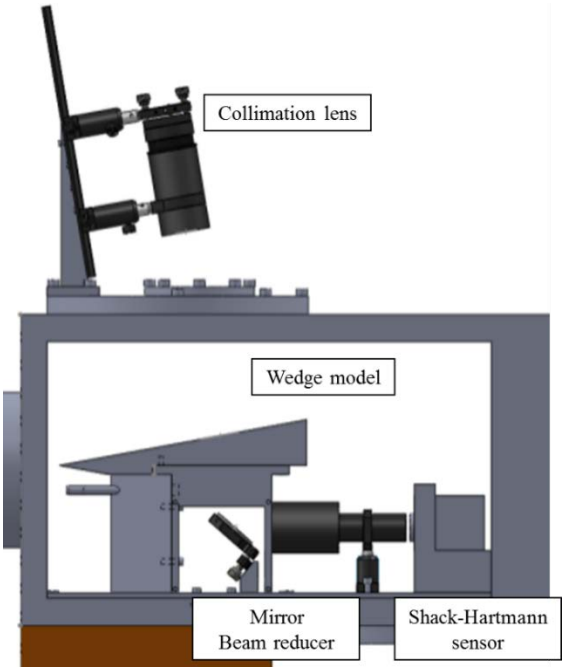

Figure 2.7 Schematic diagram of aero-optics model in shock tunnel test section.

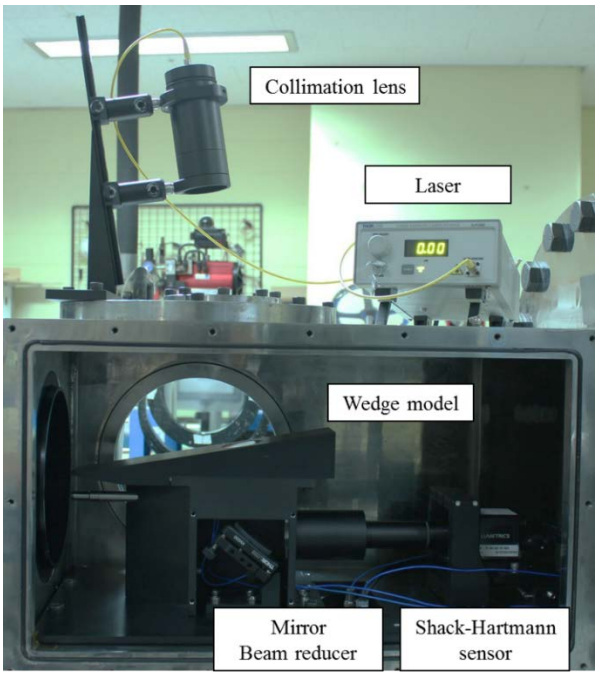

Figure 2.8 Aero-optics model in shock tunnel test section.

2.2.1 Laser

Laser is the object which optical sensor capture and analyze optical aberration induced by flow field. Power and wavelength of laser is selected considering specification of the optical sensor. Also aero-optical characteristics depends on wavelength of the laser. In this thesis, diode laser with 635 nm wave length (Thorlabs, S1FC635) is used. The laser is continuous type and maximum power is 2.5 mW. During the experiment laser power is adjusted around 0.01 mw, since Shack-Hartmann sensor is saturated at higher power. Optical fiber is connected to the laser and transfers the laser to adequate place. Due to the flexibility of optical fiber, limitation for a place to put laser and collimation lens is lessen. Optical fiber is connected to an adapter at collimation lens tube system.

2.2.2 Optical components

Optical components are designed to modify laser source to desired conditions. Optical components are categorized to three parts as collimation part, beam guiding part and beam reducer part. Collimation part produce plane wave with size that is adequate for experiment. Figure 2.9 is schematic diagram of collimation part. It is composed of a collimation lens and point source. Point source is the end of fiber optics adapter connected to optical fiber. Since point source at the focal point of convex lens becomes plane wave, convex lens is selected for collimation lens fiber optics adapter is placed at focal point. Output from the point source has certain angle of beam divergence. Thus distance from the lens and focal point affects output beam size. In the experiment achromatic lens is selected since chromatic aberration will be reduced and focuses beam better than singlet lens. Focal length of the collimation lens is 100 mm and diameter is 50.8 mm. Output beam diameter in this collimation system is around 40 mm. Collimation lens and fiber optics adapter is mounted at lens tube system to increase optical components alignment quality. Especially fiber optics adapter is mounted at distance adjustable lens tube system to adjust position and improve plane wave quality.

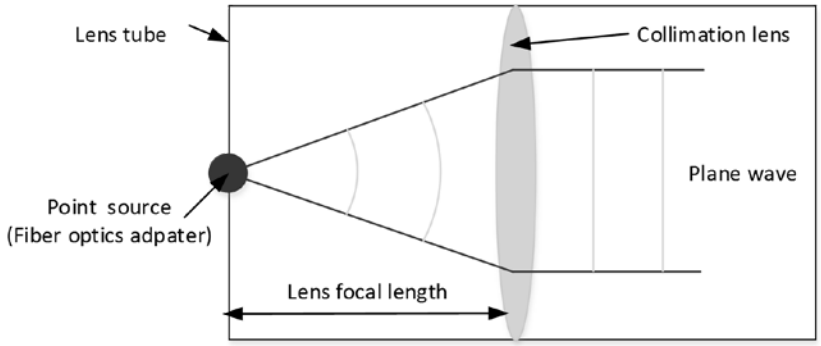

Figure 2.9 Schematic diagram of collimation part.

Collimation lens tube system is mounted on the rail which is mounted on the wedge structure as figure 2.10. Angle of incidence of the laser to the model is fixed by wedge structure angle. To minimize the refraction generated by model window, angle of incidence is fixed to be perpendicular to the wedge model. Angle of wedge structure is same as wedge model, which is 10 ° .

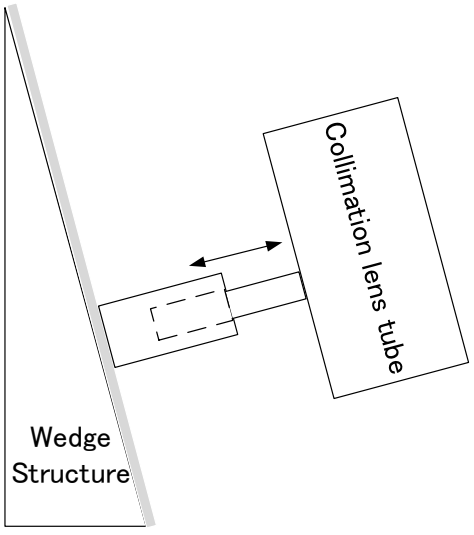

Figure 2.10 Collimation lens tube mounted on wedge structure.

Mirror is installed after model window to change laser angle and guide laser to optical sensor. Since incidence laser angle is fixed by wedged structure, mirror angle is also fixed by wedged support. Mirror mount has tilt adjusting screw but only small angle is adjustable.

Beam reducer reduces test beam size smaller than optical sensor aperture. Beam expanding and reducing makes it available to investigate bigger region of flow field and electromagnetic wave interaction. Schematic diagram of the beam reducer is as figure 2.11. Beam reducer consists of two convex lenses. Distance between two convex lenses is sums of each focal length. Reduction ratio of beam size depends on the focal length ratio of the lenses. Output beam size of beam reducer can be calculated by following equation:

$$\mathbf{D}_{output} = \mathbf{D}_{input} f_2 / f_1 \quad . \tag{2.6}$$

D_{output} is size reduced beam diameter, D_{input} is incidence beam diameter, f_1 is focal length of lens1 and f_2 is focal length of lens2. Usually f_2 is smaller than f_1 for beam reducer. f_1 is selected as 100 mm and f_2 is selected as 30 mm. Diameter of lens1 is 50.8 mm, which is same as collimation lens, and diameter of len2 is 25.4 mm. Incidence beam is reduced by 0.3. As in collimation lens, achromatic lens is used to minimize chromatic aberration and increase focusing performance. Also beam reducer lenses is mounted at lens tube system for simple alignment. To reduce process of optical component alignment, beam reducer lens tube system is connected with optical sensor aperture. Thus position of beam reducer and tilt of optical sensor is fixed.

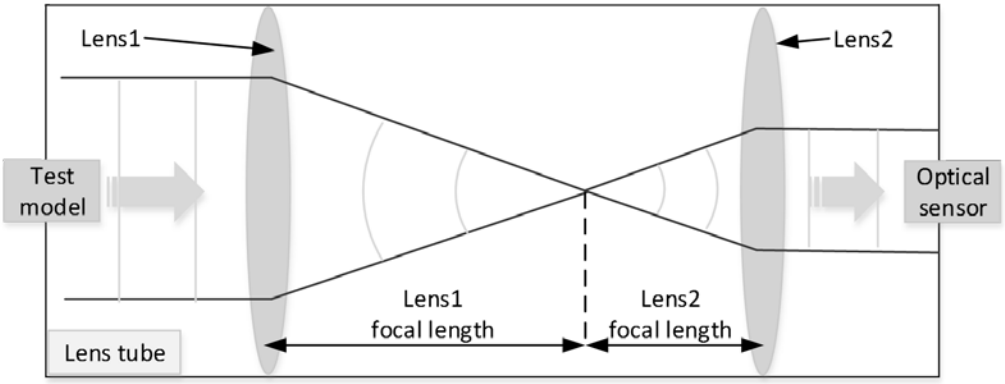

Figure 2.11 Schematic diagram of beam reducer.

2.2.3 Sensor

Pressure sensor

Pressure sensor is installed on the model to identify flow condition for every experiment. Piezoelectric type pressure sensor (PCB, 113B28) is used. Since test time is no longer than 5 msec, decay of signal as time passes is not considered. Two pressure sensor is used on aero-optics model. One is installed on the model surface and another is installed on pitot tube, which is installed beneath wedge model.

Shack-Hartmann sensor

Shack-Hartmann sensor is one of optical sensor that measures wavefront slope and intensity of incident beam. As in figure 2.12, Principle of Shack-Hartmann sensor is simple. Shack-Hartmann sensor consists of a lenslet array and a CCD. Incident distorted wave is divided to each lens of the lenslet and focuses to a point. Since CCD is placed at the focal length of the lenslet array, image of each focused point is captured with CCD. From captured image, position and intensity of the point is analyzed. Comparing the image with reference image, which is usually image of plane wave captured before each measurement, position difference and intensity difference is obtained. Position difference of focused point is wavefront slope at

corresponding lens of the lenslet array. From wavefront slope matrix at each point, wavefront is reconstructed using various method. Depending on the reconstruction method, obtained wavefront is different. In this thesis, wavefront reconstruction is conducted with modal method using Zernike polynomial. Since Shack-Hartmann sensor measures difference from reference data, only optical aberration is obtained from results. In other words, effect of aberration induced by optical system itself is neglected during measurement.

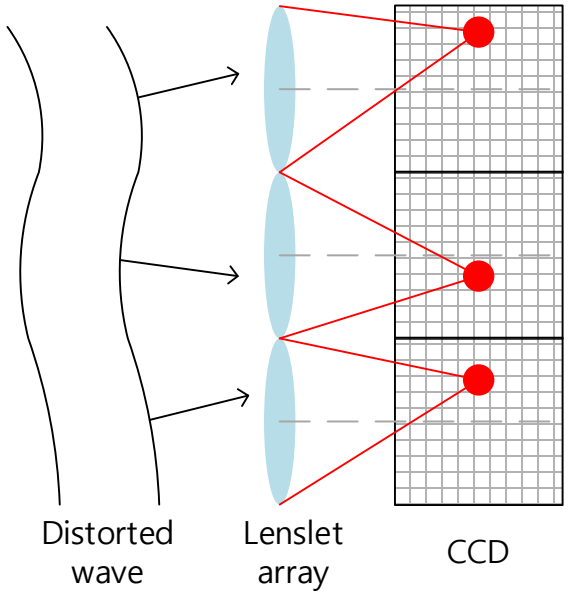

Figure 2.12 Principle of Shack-Hartmann sensor.

Shack-Hartmann sensor from Lumetrics (Model: CLAS-XP) is used for experiment. Data acquisition and analysis software is also provided from Lumetrics. Frame speed of Shack-Hartmann sensor is 30 hz and shutter speed in experiment is 0.025 ms. Since interval between each frame is 33 msec, only one frame is captured during shock tunnel test time.

Figure 2.13 Shack-Hartmann sensor (Lumetrics, CLAS-XP).

2.2.4 Model

Model part consists of test model and strut. Figure 2.14 is schematic diagram of model and figure 2.15 is its image. Test model introduce flow phenomena which is interest of the research to flow field. Wedge model with 10˚ angle is used to introduce oblique shock wave to hypersonic flow field. Below the wedge is also wedged with same angle to avoid complicated flow phenomena and generate designed oblique shock on top. Thickness of the model is 66 mm and height is 50 mm. Window for laser beam to pass through is installed on the surface. Diameter of the model window is 45 mm and material is pyrex. Strut holds the test model and secures optical components inside the model. To adjust optical components inside strut, each side of strut is able to open. Front of stut is wedged to avoid bow shock generated at the front. Pitot tube is installed beneath the test model and on front of the strut. Position of pitot tube is considered not to affect flow field on the wedge model. Pressure hole is placed on surface of the wedge model before the model window to study pressure after the oblique shock.

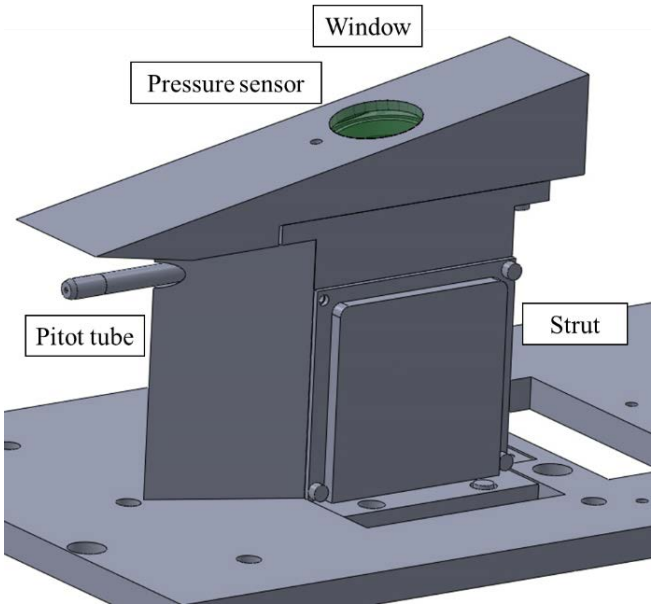

Figure 2.14 Schematic diagram of test model installed on strut.

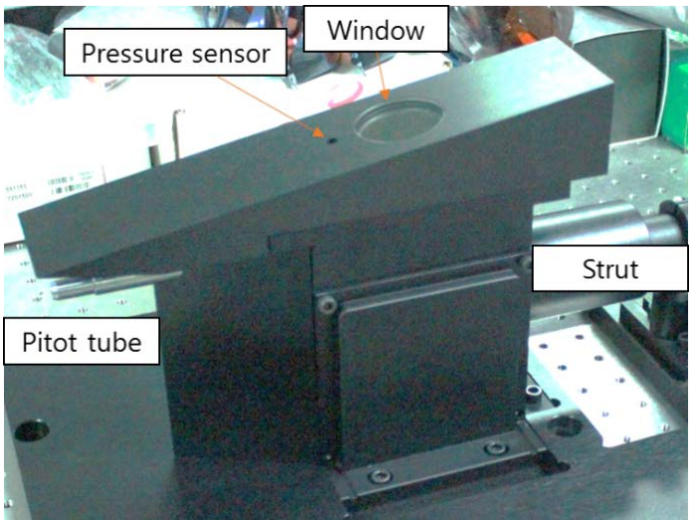

Figure 2.15 Test model installed on strut.

2.3 Measurement

2.3.1 Aero-optics measurement

Shack-Hartmann sensor acquires near-field wavefront data. Wavefront tilt is obtained from near-field wavefront. Near-field wavefront data is converted to far field data, which is called Point Spread Function (PSF). Figure 2.16 is PSF of typical aero-optics experiment result. PSF represents the image of the light source at far distance. From PSF, Bore sight error (BSE) and Strehl ratio is calculated. BSE is defined as displacement of peak intensity of the PSF and Strehl ratio is defined as ratio of peak intensity. Strehl ratio also represents quality of total optical system. Reference data for each experiment is captured after making vacuum state in the test section and before driver gas injection. Experiment data is acquired during test time of shock tunnel, which has steady shock wave formed on the wedge model and steady pressure at pitot tube.

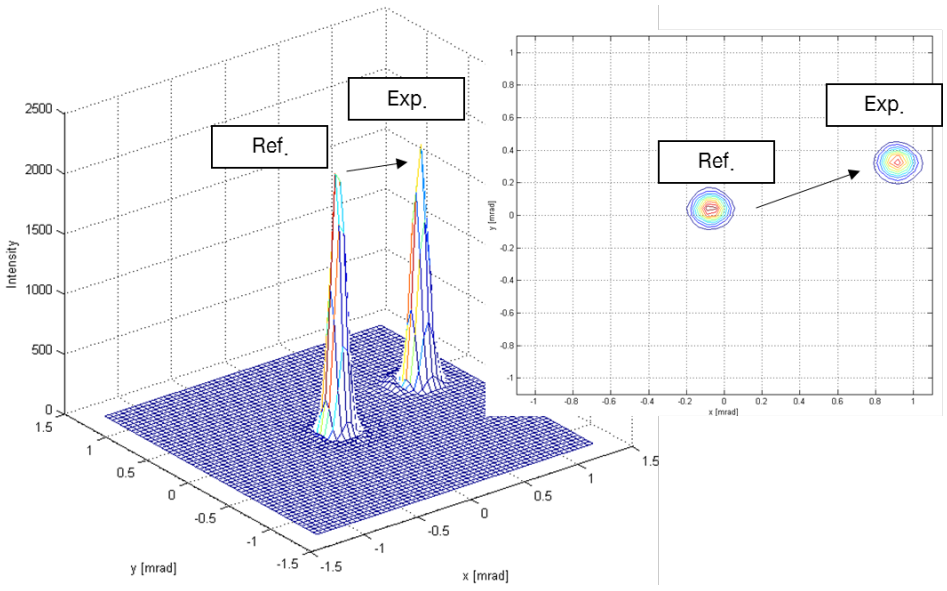

Figure 2.16 Point Spred Function of tare and expreiment data.

Since BSE obtained from the Shack-Hartmann sensor is defined as angle at the lens array, it should be converted to BSE defined as angle at window as in figure 2.17. Window is selected as a standard to maintain same standard among other models. Process of converting BSE is as in the following. First, BSE obtained from the sensor (α_s) is converted to distance on the CCD (B). Since α_s is in radian units, B is obtained by multiplying focal length of the lens array (f_{La}):

$$\mathbf{B} = \mathbf{f}_{\boldsymbol{La}}\boldsymbol{\alpha_s} \ . \tag{2.7}$$

If there is a beam reducer between the Shack-Hartmann sensor and the model window, focal length ratio of the lenses in the beam reducer should be multiplied to magnify the distance B. Magnified distance B_m is derived from following equation:

$$\mathbf{B}_{\boldsymbol{m}} = \boldsymbol{f_1/f_2 B} \ . \tag{2.8}$$

Length of distance between window and CCD sensor can be calculated from the drawing and measured directly. When there is the beam reducer, sum of the focal length of the beam reducer should be subtracted from the distance L, since it is already taken account while B_m is calculated. Finally, converted BSE α_c is calculated by following equations:

$$\text{(Without beam reducer)}\boldsymbol{\alpha_c} = \mathbf{arctan}\,\mathbf{B}/\boldsymbol{L} \ , \tag{2.9}$$

$$\text{(With beam reducer)}\boldsymbol{\alpha_c} = \mathbf{arctan}[\boldsymbol{B_m}/(\boldsymbol{L - f_1 - f_2})] \ . \tag{2.10}$$

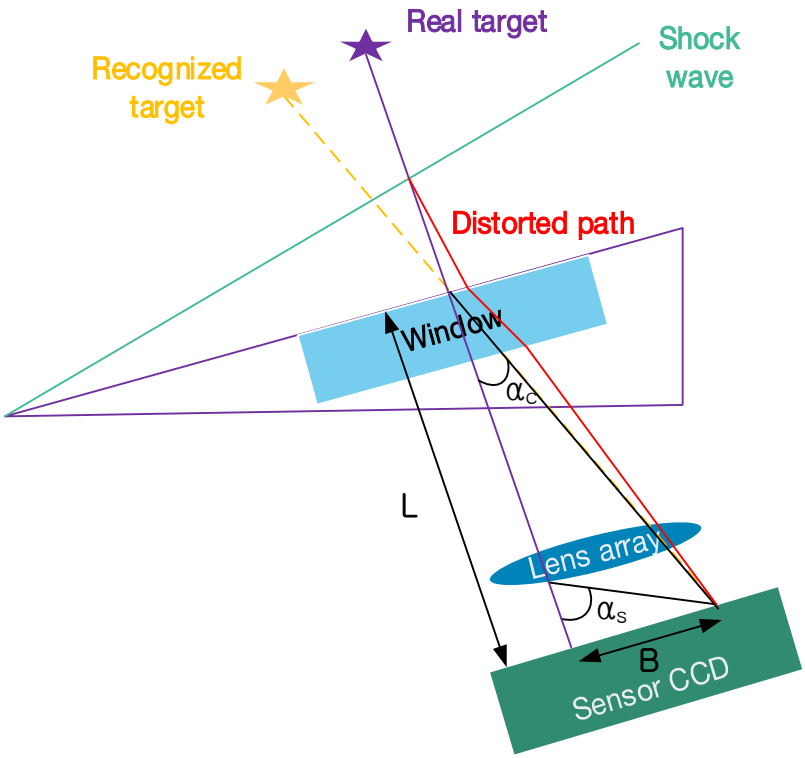

Figure 2.17 Bore sight error conversion diagram.

In this thesis, distance between center of model window and center of mirror inside the strut is 102.05 mm, center of mirror and Shack-Hartmann sensor aperture is 206.26 mm. Distance between sensor aperture and lens array is 13 mm. Distance between lens array and CCD is 4.59 mm, which is same with lens array focal length. Calculating these length, L can be obtained as 195.9 mm. Focal length of the lens in beam reducer is 100 mm, 30 mm.

2.3.2 Hypersonic flow field measurement

Flow visualization image of wedge model is obtained and pressure is measured to study flow field characteristics. Shadowgraph or schlieren technique is used for flow visualization. Figure 2.18 is schematic diagram of shadowgraph technique. Schlieren has similar set up, except knife edge is added on front of the lens before high speed camera. Because of spatial problem, Z-type shadowgraph or schlieren technique is used. Xenon lamp is used as light source and high speed camera (Phantom, v710) is used to capture images. Maximum frame rate of high speed camera is around 700,000 fps and frame rate during aero-optics experiment is around 25000 fps. Focal length schlieren mirrors are 2540 mm.

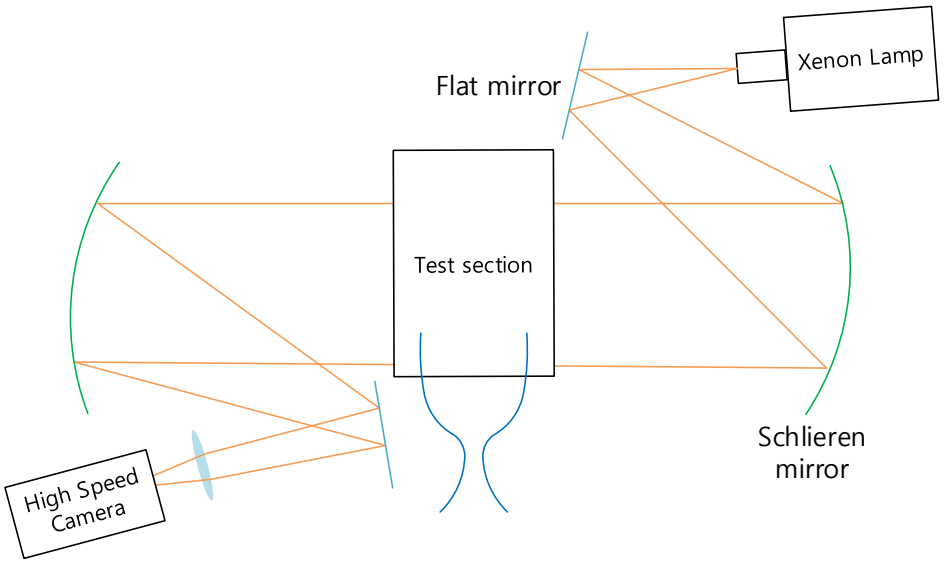

Figure 2.18 Schematic diagram of shadowgraph technique.

Oblique shock wave angle is measured from visualization image. Figure 2.19 is diagram of oblique shock wave formed on the wedge. Wedge angle, oblique shock wave angle, free stream, Mach number has following relation, which is called θ-β-M equation[4]:

$$\tan\theta = \cot\beta \frac{M_a^2 \sin^2\beta - 1}{\frac{\gamma+1}{2}M_a^2 - (M_a^2 \sin^2\beta - 1)} \quad . \tag{2.11}$$

θ is wedge angle, β is oblique shock angle and M_1 is free stream Mach number. From given θ and measured β, free stream Mach number is calculated.

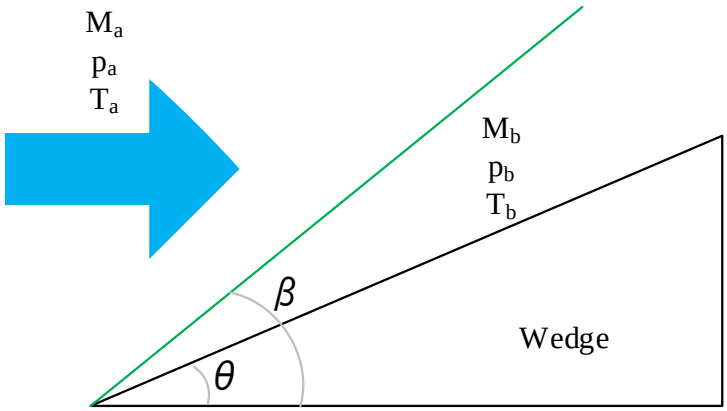

Figure 2.19 Diagram of oblique shock wave on the wedge.

Simultaneously with flow visualization of wedge, stagnation pressure is measured using pitot tube to obtain stagnation pressure loss throughout the nozzle. Diagram of flow before the pitot tube is as in figure 2.20. Bow shock wave forms in front of the pitot tube and pitot tube measures stagnation Mach number behind the shock. Bow shock is assumed to be normal shock on region near pitot tube pressure tab. Then stagnation pressure ratio (p_{0b}/p_{0a}) and free stream Mach number (M_a) has following relation[4]:

$$\frac{p_{0b}}{p_{0a}} = \left[\frac{\frac{\gamma+1}{2}M_a^2}{1+\frac{\gamma-1}{2}M_a^2}\right]^{\gamma/(\gamma-1)} \left[\frac{1}{\frac{2\gamma}{\gamma+1}M_a^2 - \frac{\gamma-1}{\gamma+1}}\right]^{1/(\gamma-1)} . \tag{2.12}$$

p_{02} is measured from pitot tube and one value between M_a and p_{0a} should be known

to determine another. M_a is obtained through flow visualization of the wedge and p_{0a} is calculated from equation 2.12. Calculated p_{0a} is compared with stagnation pressure at nozzle inlet, which is measured in driven tube. Thus stagnation loss during flow expansion inside the nozzle is acquired.

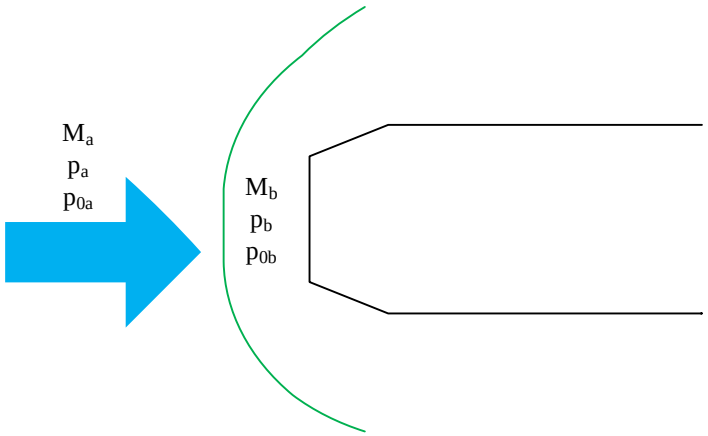

Figure 2.20 Diagram of bow shock in front of pitot tube.

Pressure distribution of nozzle exit flow is measured with pitot rake to validate the nozzle uniformity. Mach number distribution is obtained by calculating p_{0a} from multiplication of driven tube measured stagnation pressure and nozzle stagnation pressure loss ratio. Since diameter of nozzle exit is different, different pitot rake is used for each nozzle. Pitot rake designs are similar except pitot rake support. Same pitot tube installed at aero-optics model is used and total 5 pitot tubes are used for each pitot rake. For conical nozzle, pitot rake support has 5 holes to install pitot tube. Middle pitot tube is at center of the conical nozzle and other pitot tube is placed for every 30 mm. Maximum available measurement diameter is 120 mm. For contoured nozzle, pitot rake support has 10 holes to install pitot tube. Axis between two middle holes (5^{th} and 6^{th} hole from the top), is at center of the contoured nozzle. Interval between each holes is 20 mm and maximum available measurement diameter is 180 mm. 5 pitot tubes are installed on any 10 holes depending on test condition. At first, contoured nozzle flow symmetry is evaluated by installing pitot tube symmetrically

to the nozzle axis (such as 2^{nd}, 3^{rd}, 5^{th}, 7^{th}, 9^{th} from the top). Then pressure distribution is measured at top half of the nozzle. Results for top half of the nozzle is only presented in this thesis.

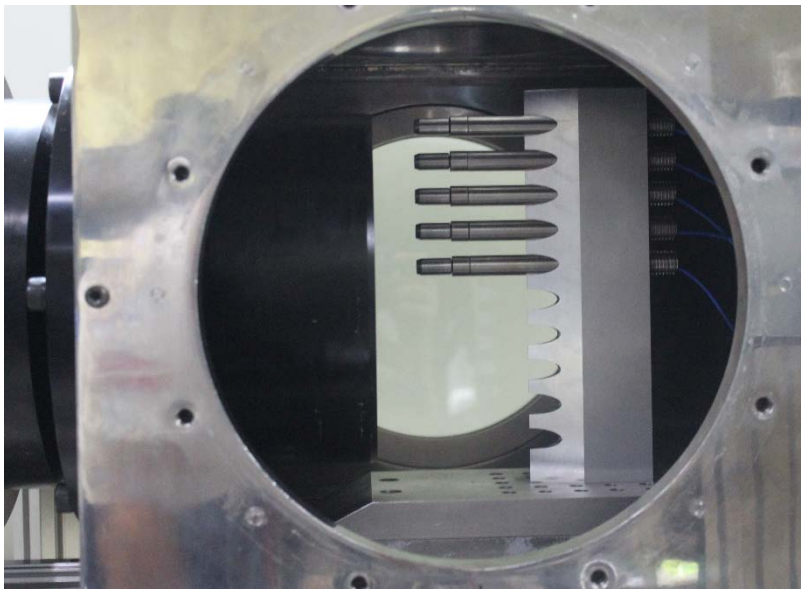

Figure 2.21 Pitot rake inside shock tunnel test section.

2.3.3 Measurement trigger system

Trigger is important since Shack-Hartmann sensor can be acquired once and visualization image acquisition should be synchronized with Shack-Hartmann sensor. Total Data acquisition (DAQ) system is triggered by pressure rise (or voltage rise) measured at driven tube. Moving shock generated from diaphragm passes the pressure sensor on the driven tube and rises voltage signal from the sensor. Pressure sends the signal to the DAQ acquisition board and triggers other pressure sensors which are connected to same DAQ board. Simultaneously, voltage signal from the pressure sensor go to delay generator. Delay generator (DG-535) generates time interval between signal from pressure sensor and Shack-Hartmann sensor trigger

signal. Time interval is selected to trigger Shack-Hartmann sensor at steady flow region inside test section as in figure 2.23. In figure 2.23, pressure sensor triggered pressure sensors at 0 msec, and Shack-Hartmann sensor is triggered at 9.8 msec later. Many experiments is conducted to determine the time interval. Trigger signal of Shak-Hartmann sensor should be TTL signal (0V<low voltage<0.8V; .4V<high voltage<5V) with minimum 50 ns interval of high voltage. DG-535 is adjusted to output ne pulse of square wave with 100 ns interval of high voltage. DG-535 output signal triggers Shack-Hartmann sensor and go to camera trigger box. Camera trigger box modifies the signal adequate for high speed camera trigger. Camera trigger box changes entered signal to rise signal. Voltage rises to 5V and sustain for several seconds. At each experiment, trigger time of Shack-Hartmann sensor and high speed camera is recorded.

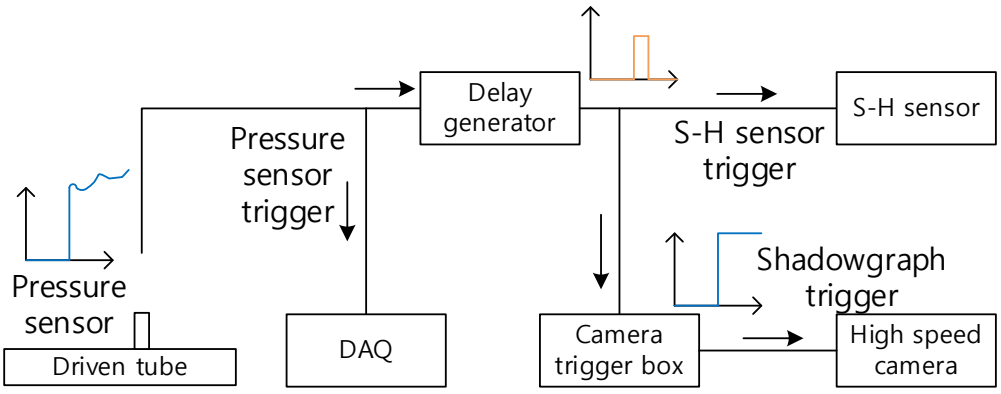

Figure 2.22 Block diagram of measurement trigger system.

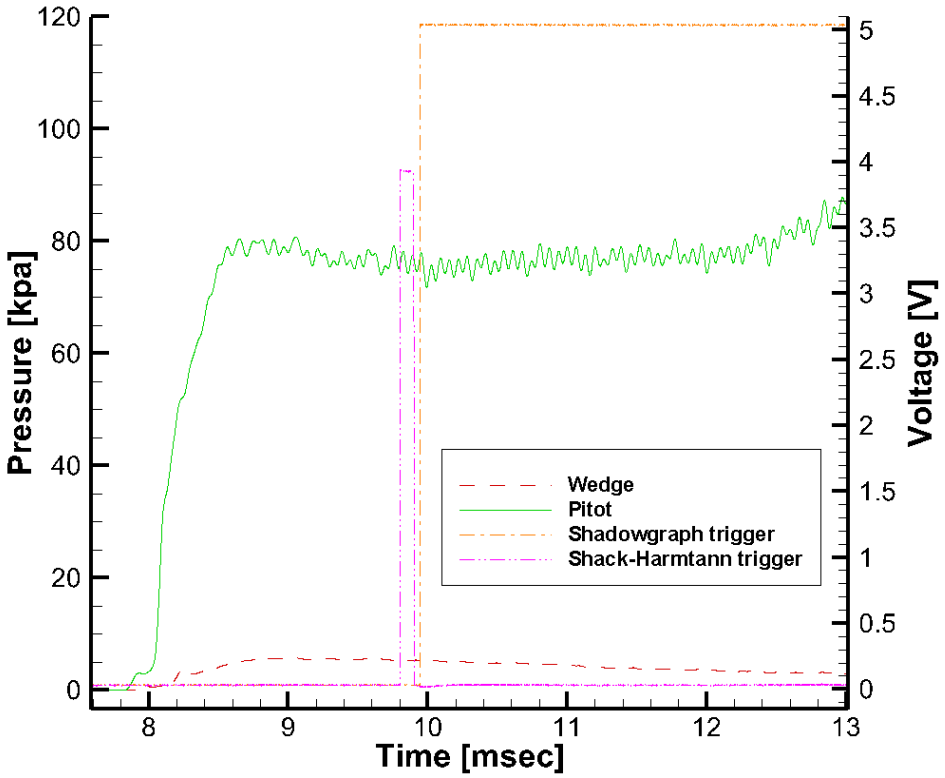

Figure 2.23 Trigger time of flow visualization and Shack-Hartmann sensor.

3. Experiment results

3.1 Aero-optical characteristics in static flow

Aero-optics experiments are held at static flow to understand the principle and validate the Shack-Hartmann sensor. Figure 3.1 is configuration of aero-optics experiment on optical table. 635 nm diode laser is used as a light source and collimation lens produces plane wave. Plane wave propagates through test object and Shack-Hartmann sensor measures phase and intensity of the laser. Two experiments are conducted using different test object. First experiment is conducted with wedged window. Wedged window refracts laser to certain degree which can be calculated through Snell's equation. Second experiment is conducted with hot gun. Heat induced aero-optical aberration around hot wire is observed.

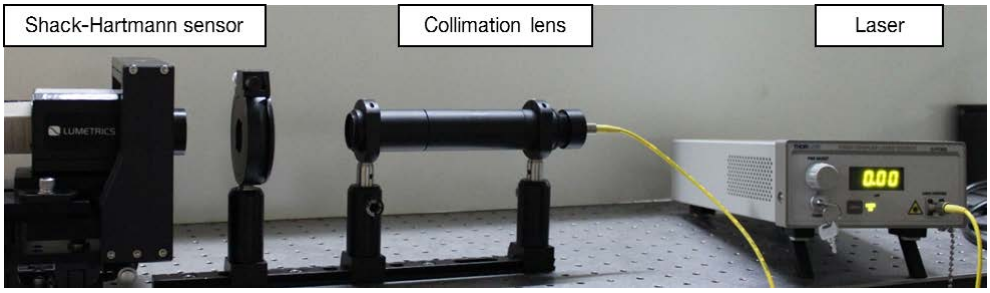

Figure 3.1 Configuration of static flow aero-optics experiment.

3.1.1 Experiment using wedged window

Schematic diagram of laser propagating through wedged window is as figure 3.2. Wedged window is typical cylinder window with inclination on one side. Wedged window tilts the laser to designed angle. Snell's law is used to calculate the angle of refraction. Since maximum tilt that sensor can measure is ±6.7 mrad, wedged window with wedged angle 0.5˚±0.167˚ is selected. Material of the window is N-BK7 which has refractive index 1.5168. Assuming air refractive index is 1, refractive

angle of the laser is 3.005 mrad ~ 6.011 mrad.

Wedged window is installed between collimation lens and Shack-Hartmann sensor. Since diameter of the wedged window is 25.4 mm, 2 convex lens is used after collimation lens to scale down the laser beam size. Diameter of the lenses is 25.4 mm and focal length of the collimation lens is 45 mm, focal length of first beam reducer lens, which is near the collimation lens, is 50 mm, and focal length of final lens is 30 mm. After the final lens, beam diameter is less than sensor aperture. Wedged window is mounted on the 360˚ rotation lens mount. Laser is measured for every 30˚ degree rotated, to validate the Shack-Hartmann sensor 2-D measure performance.

The result is presented at figure 3.3. Blue dots are measured points for every 30˚ rotation and red circle is averaged value of blue points. Average value is 3.259 mrad, which is within the range of the calculated refraction angle. Every blue dots are on red circle, which means same tilt is measured through 360˚ rotation. From the results Shack-Hartmann sensor measures 2-D properly.

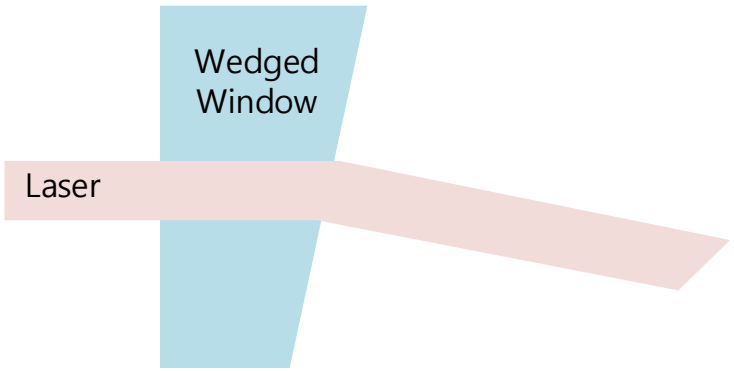

Figure 3.2 Schematic diagram of laser propagation through laser.

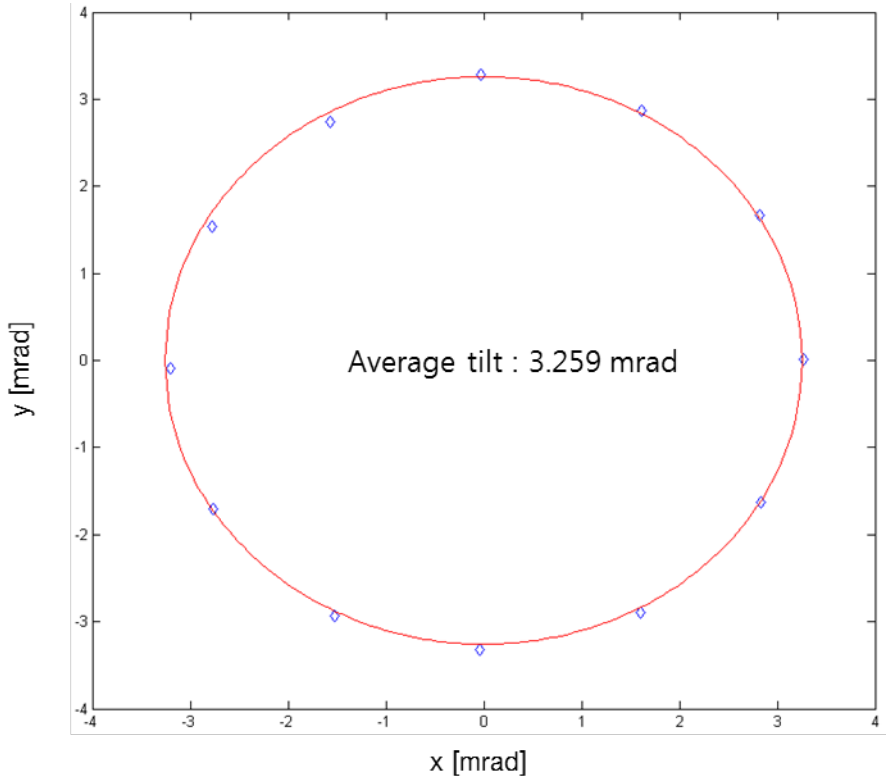

Figure 3.3 Tilt measured after wedged window.

3.1.2 Experiment using hot wire

Aero-optical phenomena around hot wire (Ni-Ct wire) is observed. Electricity is applied to hot wire and heat is generated. 100 mm lens is used as collimation lens and beam reducer isn't used to study detailed phenomena around hot wire. Reference laser data is obtained with no wire on the beam path, and then hot wire is installed to conduct experiment. It is because hot wire transforms due to applied electricity. Electricity is provided with power supply (Agilent U8001A). Voltage is controlled and corresponding current is displayed on the supply. Experiment is performed at three power 0.06 W, 1.5 W, 6.1 W.

Wavefront result at 1.5 W is presented as figure 3.4. In figure 3.4, P-V OPD value change near the hot wire as electricity is applied. RMS tilt and RMS OPD value is

presented in figure 3.5. Tilt is produced at y axis, which means heat is transferred to y direction. As power increase, heat produced on the wire is also increased. RMS tilt and RMS OPD value also increase as power increase. Thus optical aberration increased as heat is increased.

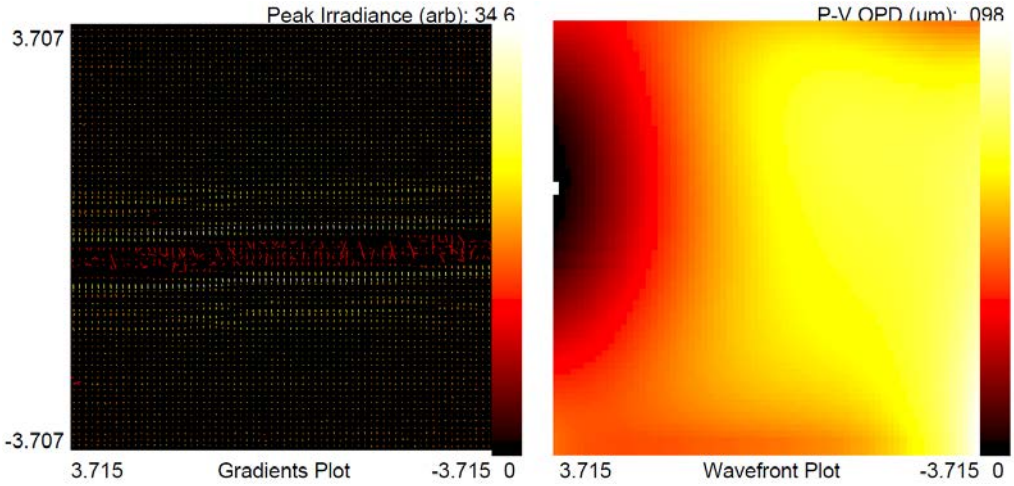

a) Aero-optical characteristics near hot wire with no electricity.

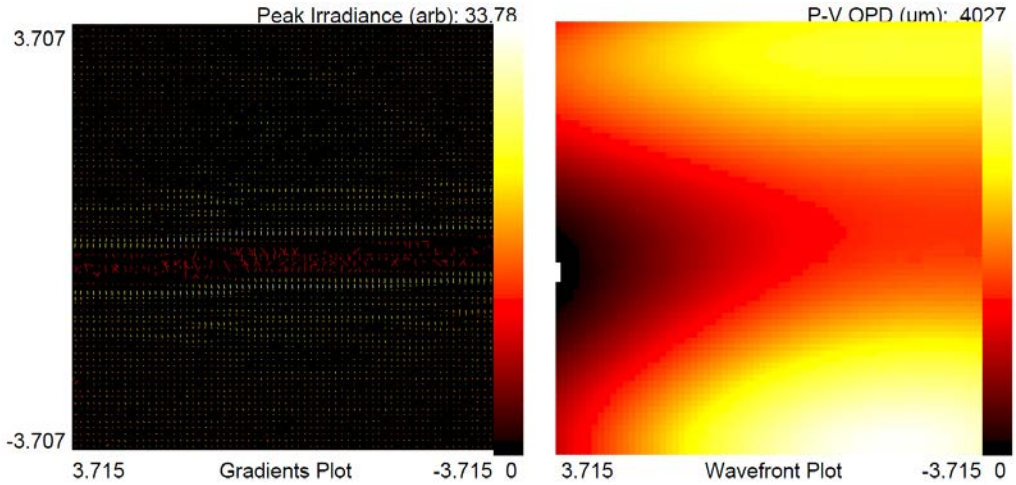

b) Aero-optical characteristics near hot wire with 1.5 W electricity.

Figure 3.4 Aero-optical characteristics near hot wire (PV-OPD).

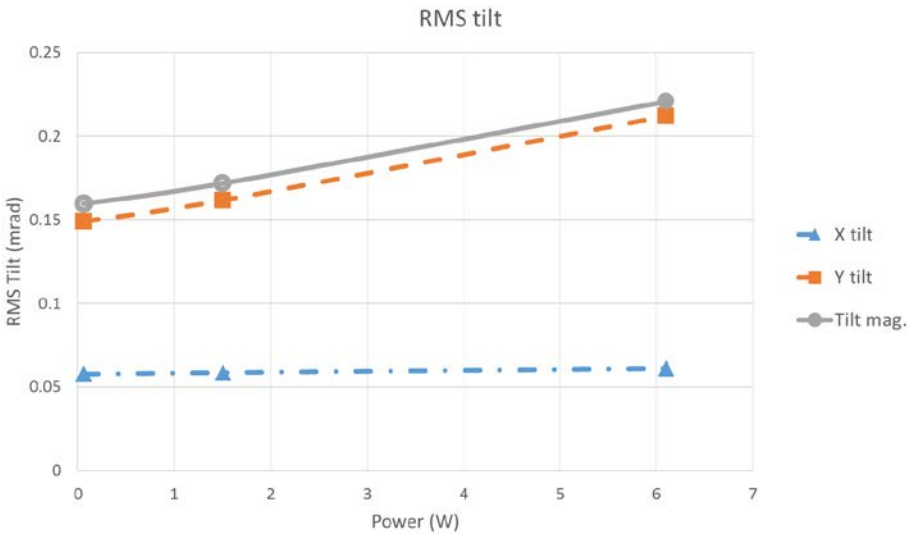

a) RMS tilt depending on power consumed by hot wire.

b) RMS phase depending on power consumed by hot wire.

Figure 3.5 Aero-optical characteristics depending on power consumed by hot wire.

3.2 Hypersonic flow field characteristics

3.2.1 Shock tunnel performance validation

Shock speed and test time is measured to validate shock tunnel performance. Shock speed is measured using pressure sensors on the driven tube. Total 6 piezoelectric PCB sensors are installed on the driven tube as in figure 3.6. For p_1=0.26 Mpa and p_4=4.09 Mpa, pressure measured at driven tube is as in figure 3.7. As Shock wave generated at 1st diaphragm propagates through driven tube, sensors rise suddenly when shock wave pass by. Shock speed is measured by dividing distance between each sensor with interval between each rise of sensor. From the result shock speed is 595.98 m/s. Through equation (2.1) and (2.2), shock speed is calculated as 610.73 m/s. Measured shock speed is smaller than calculated shock speed. However state 2 pressure measured with sensor is also smaller than calculated pressure, as 0.78Mpa and 0.90 Mpa each. Using measured state 2 pressure, shock speed is calculated as 573.09 m/s. Among these three value calculation through state 2 pressure seems to be most reliable. Because rise time of pressure sensor is different for every sensor producing error to measure shock speed and sensor that measures p4 is placed far away from driver tube having less accuracy than sensors at driven tube. Hereafter, pressure at state 2 is measured and stagnation condition of the nozzle is calculated using this pressure.

Figure 3.6 Pressure sensor on driven tube

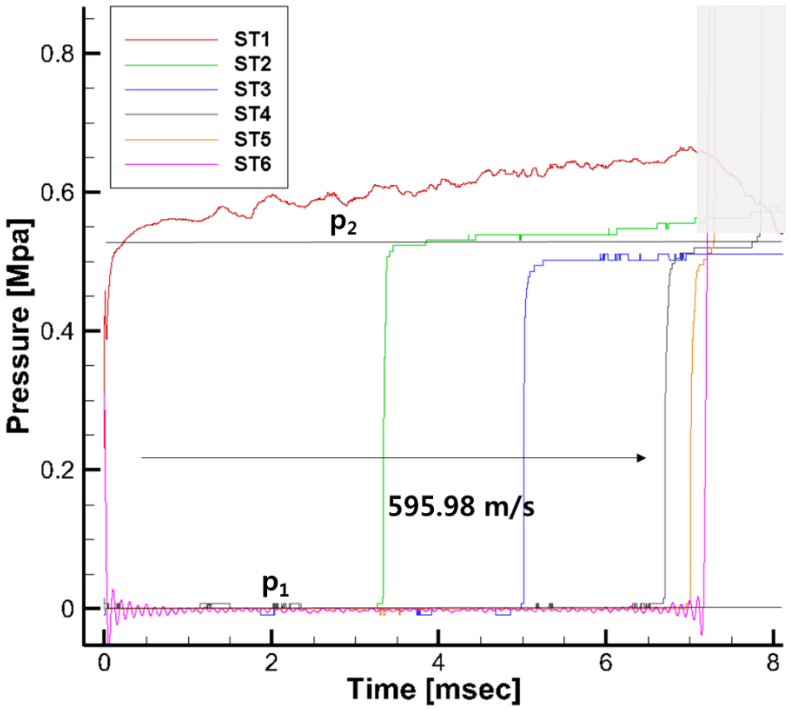

Figure 3.7 Pressure rise induced by incident shock wave in driven tube.

Test time at test section is measured simultaneously with driven tube pressure. Pitot tube is used to measure stagnation pressure at test section. From pressure measurement at the driven tube, stagnation pressure before the nozzle sustains for 3.7 msec. At test section, measured pressure result is as in figure 3.8. Steady pressure region sustained for 3.6 msec, which is similar as sustain time in the driven tube. Thus there is no loss in air volume between stagnation condition inside driven tube and test section. Test time is also long enough to obtain one frame using Shack-Hartmann sensor.

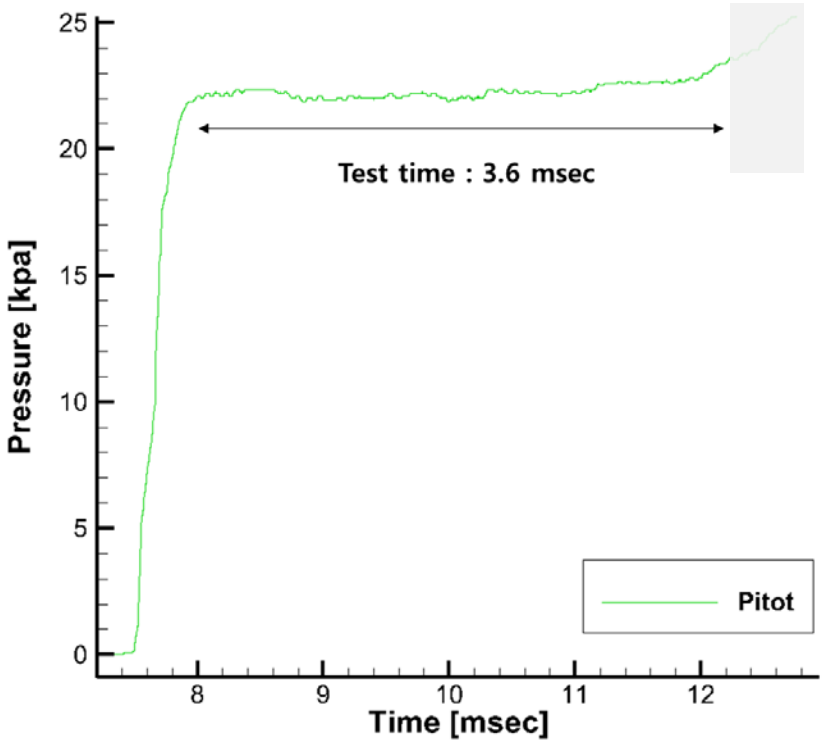

Figure 3.8 Development of shock wave (Conical nozzle, p_0=3.894 Mpa).

3.2.2 Test flow characteristics

Aero-optics wedge model and pitot rake is used to validate test flow characteristics. Schlieren or Shadowgraph image is acquired to measure oblique shock angle over wedge and test flow Mach number is obtained. Simultaneously with the visualization, stagnation pressure at the test section and stagnation pressure before the nozzle is acquired to calculate stagnation pressure loss over the nozzle. Pitot rake has series of pitot tubes which can measure stagnation pressure. Experiment is held for both conical nozzle and contoured nozzle.

Conical nozzle

Figure 3.9 shows the shock wave formation at the wedge when conical nozzle is installed at shock tunnel. It takes 240 μsec for shock wave to form over the wedge

and become stable. Thus nozzle flow is stable and test condition is achieved as soon as flow arrive at nozzle exit.

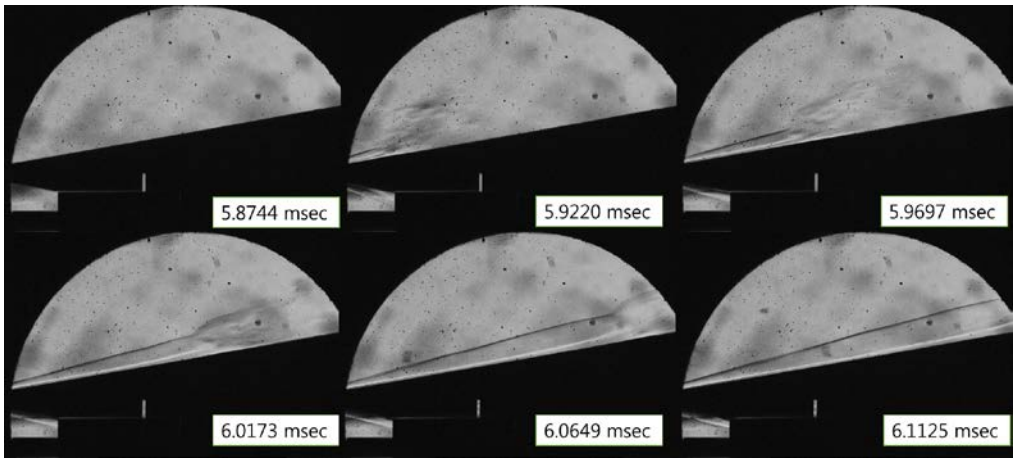

Figure 3.9 Development of shock wave (Conical nozzle, p_0=3.894 Mpa).

Visualization image of oblique shock wave over the wedge model at conical nozzle flow is obtained as figure 3.10. Measured Oblique shock wave angle is 16.6˚, which corresponds to Mach 6.8. It is similar value with designed point which is Mach 7. Stagnation pressure measured with pitot and static pressure measured at wedge surface is 67.789 kpa, 1.94 kpa each as in figure 3.11. For Mach 6.8, stagnation pressure value ratio is 0.01741. Therefore stagnation pressure at test section is 3.894 Mpa. Since p_0 measured before the nozzle is 5.37 Mpa, stagnation pressure decreased by 72%. Repeated experiment result revealed 63% average stagnation loss. Thus in this thesis, 63% loss will be considered for conical nozzle, and nozzle exit Mach is assumed to be 6.8.

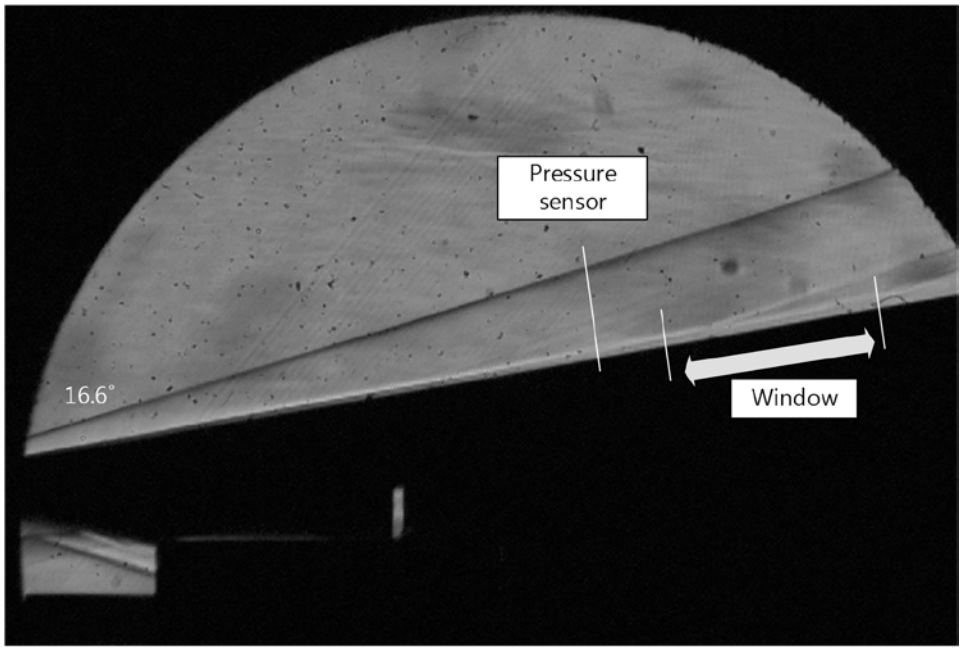

Figure 3.10 Schlieren image of wedge model (Conical nozzle, p_0=3.894 Mpa).

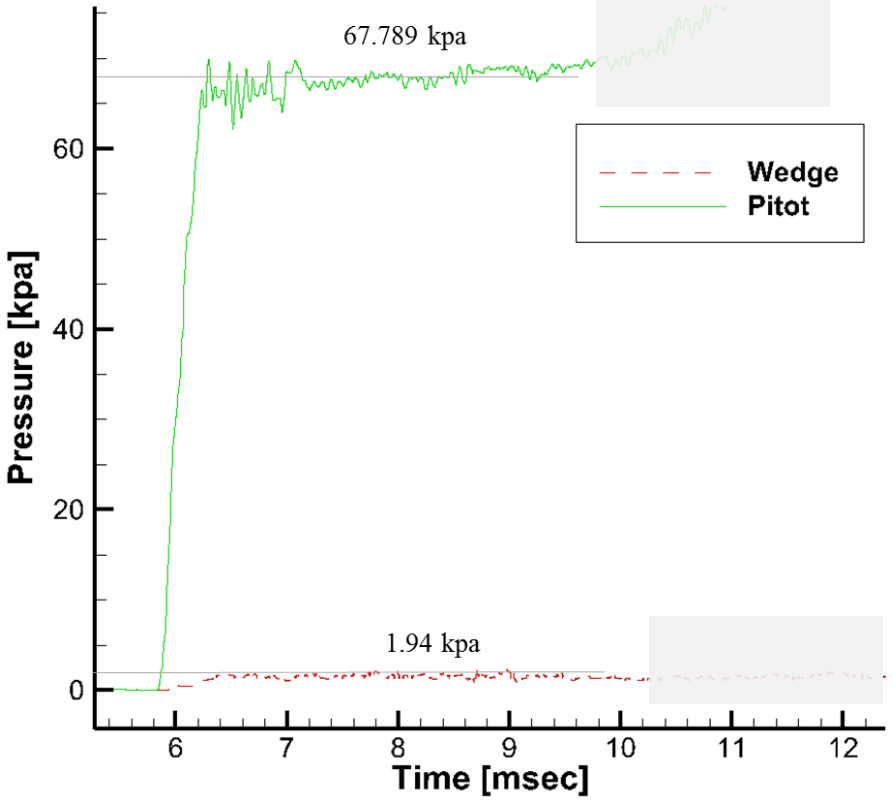

Figure 3.11 Pressure at wedged model (Conical nozzle, p_0=3.894 Mpa).

Pitot rake is used to measure stagnation pressure distribution and Mach number distribution. Test section stagnation pressure is acquired by considering 63% loss from the conical nozzle. Ratio of the stagnation pressure of test section and each pitot tube is compared to calculate Mach at each point. Results showed that pressure and Mach is quite equivalent throughout. Mach number is higher than 6.8, but error seems to occur while measuring stagnation pressure using 63% loss of the driven tube. From conical nozzle validation experiment result, 63% of stagnation pressure loss is observed and 120 mm diameter is a region where experiment can be conducted.

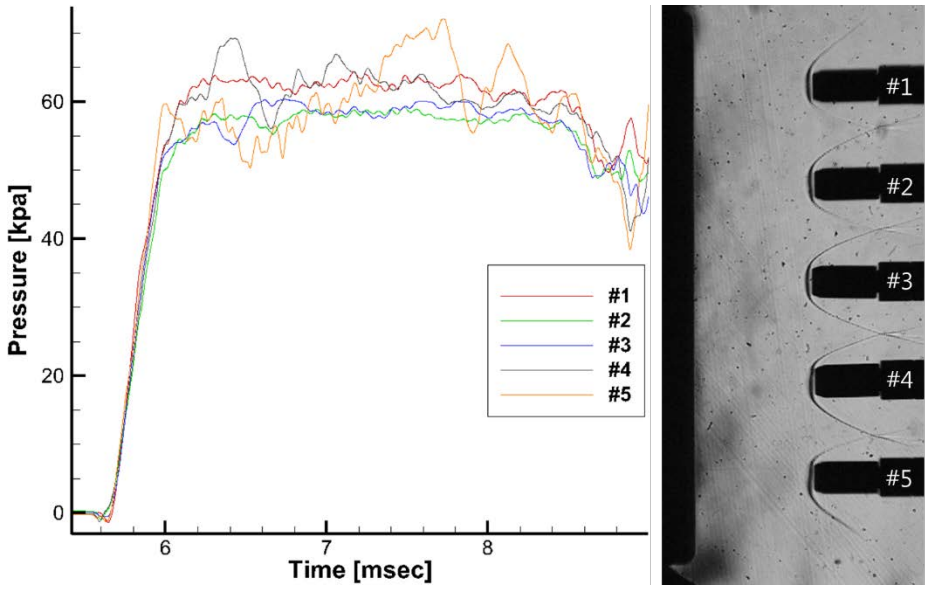

Figure 3.12 Pressure and schlieren image of pitotrake (Conical nozzle, p_0=3.849 Mpa).

Table 3.1 Pressure measured with pitot rake (Conical nozzle, p_0=3.894 Mpa).

Pitot / Result	#1	#2	#3	#4	#5
Pressure [kpa]	62.372	57.642	58.406	62.072	60.815
Mach	6.915	7.041	7.019	6.922	6.955

Contoured nozzle

Figure 3.13 shows the shock wave formation at the wedge in contoured nozzle exit flow. It takes 350 μsec for shock wave to stabilize on the wedge. Thus nozzle exit flow is stable and test condition is achieved as soon as nozzle exit flow arrive at the wedge model.

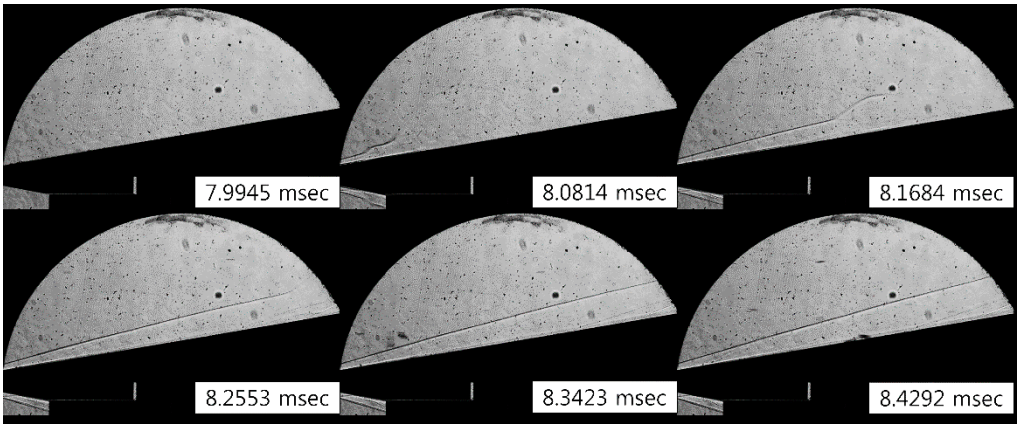

Figure 3.13 Development of shock wave (Contoured nozzle, p_0=6.13 Mpa).

Shadowgraph image of oblique shock wave over the wedge model in contoured nozzle exit flow acquired as figure 3.14. Oblique shock wave angle is measured as 16.4˚, which corresponds to Mach 6.9. It is similar value with designed point which is Mach 7. Stagnation pressure measured with pitot and static pressure measured at wedge surface is 96.331 kpa, 6.57 kpa each as Figure 3.15. For Mach 7, stagnation pressure value ratio is 0.01535. Therefore stagnation pressure at test section is 6.275 Mpa. Since p_0 measured before the nozzle is 6.13 Mpa, stagnation pressure seemed to increase by 102%. Since stagnation pressure can't increase, this seemed to be an error and stagnation pressure expanding process seemed to be isentropic. Repeated experiment result revealed similar result. Thus in this thesis, no loss will be considered for contoured nozzle, and nozzle exit Mach is considered as 7.

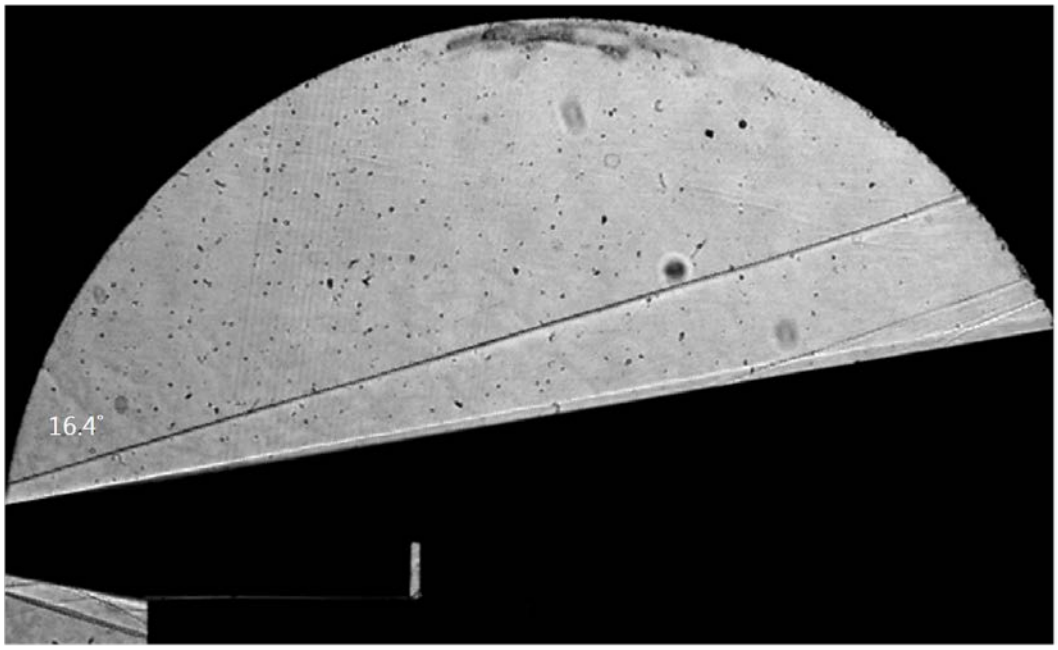

Figure 3.14 Shadowgraph image of wedge model (Contoured nozzle, p_0=6.13 Mpa).

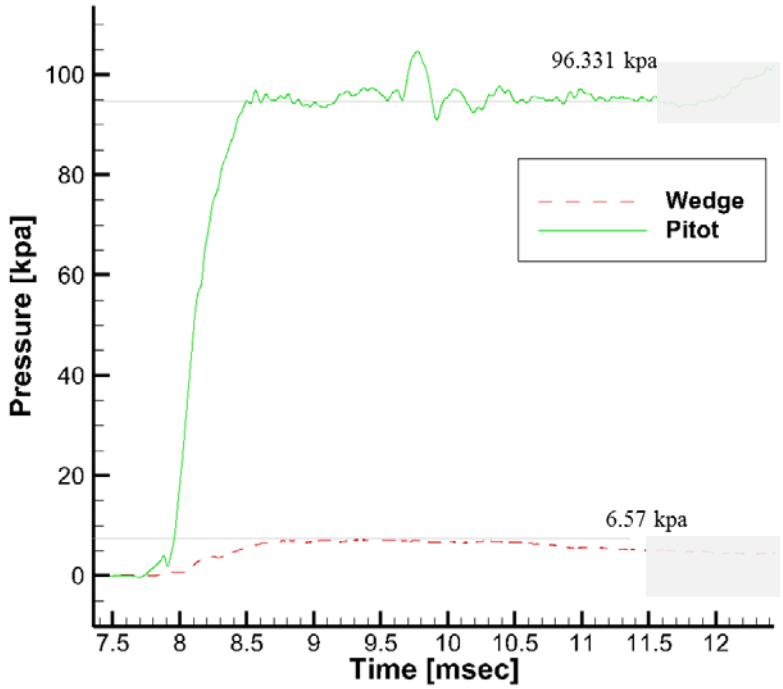

Figure 3.15 Pressure at wedged model (Contoured nozzle, p_0=6.13 Mpa).

Pitot rake is used to measure stagnation pressure distribution and derive corresponding Mach number. Test section stagnation pressure is considered to be same with nozzle inlet stagnation pressure. Ratio of the stagnation pressure of test section and each pitot tube is compared to calculate Mach at each point. Effect diameter of experiment is 144 mm, which is enough for experiment with current result.

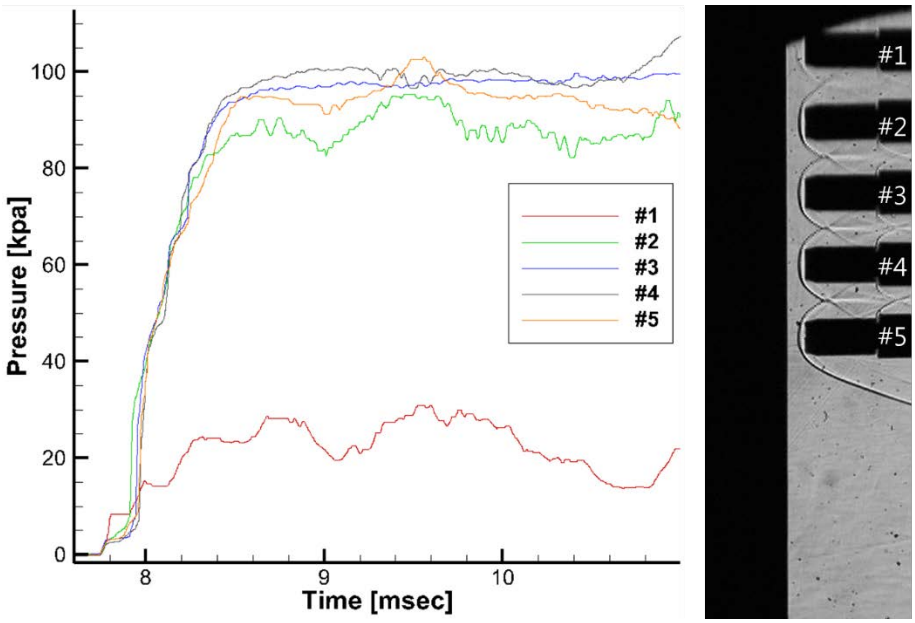

Figure 3.16 Pressure and shadowgraph image of pitotrake (Contoured nozzle, p_0=6.01 Mpa).

Table 3.2 Pressure measured with pitot rake (Contoured nozzle, p_0=6.01 Mpa).

Pitot / Result	#1	#2	#3	#4	#5
Pressure [kpa]	23.704	88.652	97.801	99.531	95.491
Mach	8.140	7.064	6.906	6.879	6.945

3.3 Aero-optical characteristics in hypersonic flow field

Aero-optics experiment in hypersonic flow is conducted for three altitude 29.1 km, 32.3 km, 38.6 km. For each altitude, pressure and temperature is as in table 3.3. Since temperature is not controllable in current system, pressure is controlled to match each static pressure. For 29.1 km, p1, which is pressure of driven tube, is 0.76 Mpa and p4 is 8.3-8.5 Mpa (pressure ratio 11), for 32.3 km p1, p4 is same with 29.1 km altitude but used conical nozzle so pressure loss is introduced. For 38.6 km, two kind of pressure ratio is used. One condition is that p1 is 0.26 Mpa, p4 is 27.5-28.5 Mpa(pressure ratio 11). The other condition is that p1 is 0.09 Mpa, p4 is 6.9 Mpa(pressure ratio 76.7) which is the case for 1.5 bigger temperature. But since there is not much difference between low temperature and high temperature, the temperature effect is neglected and two condition is considered as same altitude condition. For each experiment, wavefront information is acquired, and PSF is calculated. From PSF BSE, Strehl ratio is obtained. From wavefront information, certain tilt induced by shock wave is observed. Figure 3.17 is typical wavefront information acquired and table 3.4 is all of the aero-optics experiment data acquired with Shack-Hartmann sensor.

Table 3.3 Pressure and temperature for altitude.

Condition / Altitude	Pressure [kpa]	Temperature [K]
29.1 km	1.353	228.56
32.3 km	0.851	238.28
38.6 km	0.360	256.76

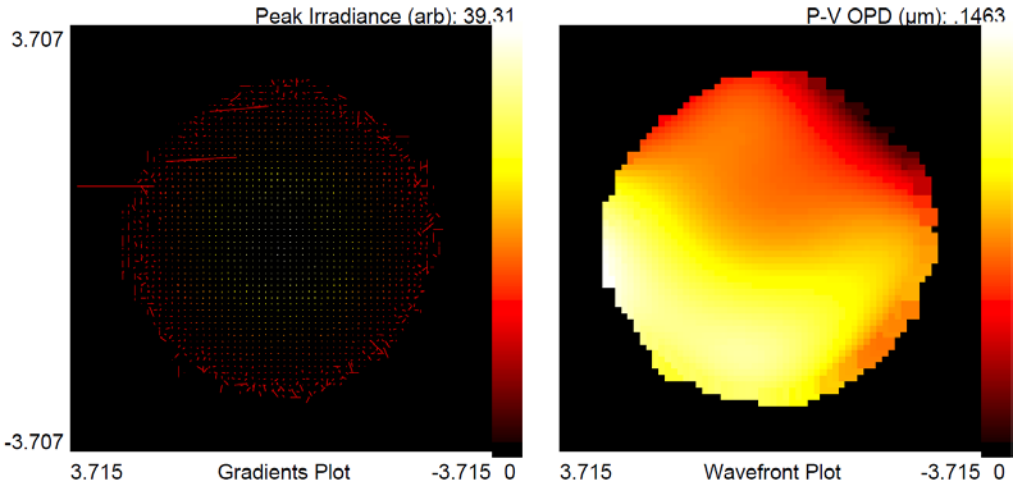

a) Irradiance and phase before shock wave formed at wedge model.

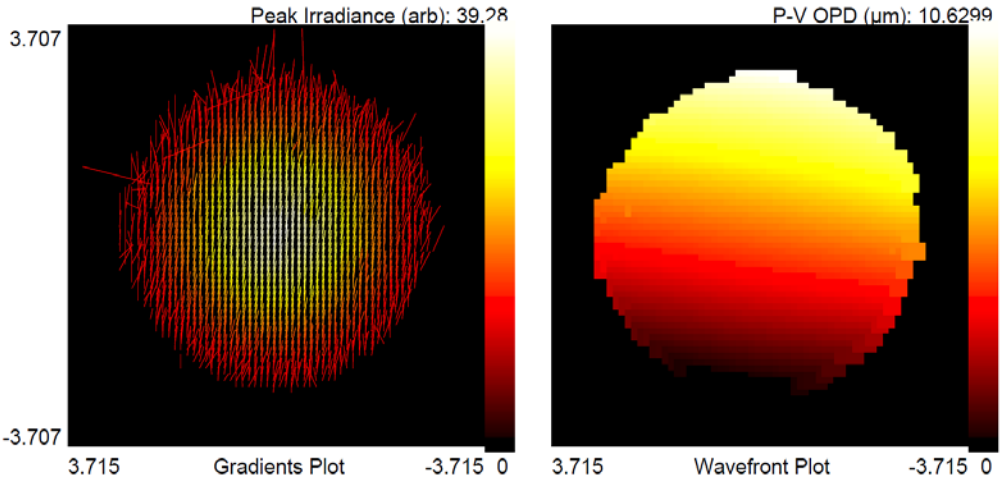

b) Irradiance and phase after shock wave formed at wedge model.

Figure 3.17 Aero-optical characteristics around wedge model

(Conical nozzle, p_0=13.612 Mpa).

Table 3.4 Aero-optical characteristics depending of stagnation condition.

Run number	Nozzle type	p_0 [Mpa]	T_0 [K]	Bore sight Error					Tilt					Strehl Ratio
				Raw BSE [mrad]		Converted BSE [µrad]			Raw Tilt [mrad]		Converted Tilt [µrad]			
				x	y	x	y	Magnitude	x	y	x	y	Magnitude	
1	Concial nozzle	3.383	352.837	-0.231	-1.654	-18.069	-129.674	130.927	-0.269	-1.789	-21.100	-140.279	141.857	0.735
2		3.528	355.475	0.585	0.139	45.859	10.881	47.132	-0.585	-0.204	-45.835	-15.992	48.545	0.930
3		3.812	367.603	1.272	-0.765	99.713	-59.969	116.357	-1.254	-0.744	-98.297	-58.354	114.313	0.839
4		1.361	403.722	1.786	0.281	139.982	22.036	141.706	-1.930	0.298	-151.322	23.321	153.109	0.743
5		1.394	403.968	0.872	0.917	68.318	71.916	99.193	-0.925	1.009	-72.530	79.081	107.305	0.682
6		1.440	412.987	0.184	0.833	14.385	65.307	66.873	-0.218	0.925	-17.074	72.481	74.465	0.780
7		1.503	673.118	0.001	-0.001	0.055	-0.055	0.078	0.003	0.002	0.197	0.172	0.261	0.939
8		1.681	719.193	1.189	1.010	93.183	79.151	122.262	-1.211	1.116	-94.960	87.450	129.092	0.778
9		1.435	655.346	-2.020	-0.142	-158.373	-11.139	158.764	2.120	-0.129	166.173	-10.127	166.481	0.684
10		1.391	650.787	-0.046	0.000	-3.590	0.008	3.590	0.049	0.016	3.865	1.251	4.062	0.970
11	Contoured nozzle	5.645	568.405	1.011	0.276	79.222	21.605	82.115	-0.952	0.330	-74.620	25.858	78.973	0.960
12		6.130	585.416	-1.929	0.873	-151.224	68.443	165.991	2.072	0.861	162.456	67.499	175.920	0.525
13		5.332	561.348	2.389	-0.046	187.244	-3.598	187.279	-2.574	-0.157	-201.786	-12.323	202.162	0.351
14		5.626	566.660	0.138	-2.113	10.802	-165.632	165.984	-0.176	-2.157	-13.796	-169.081	169.643	0.746
15		5.380	564.730	0.689	-0.459	54.011	-35.974	64.895	-0.775	-0.559	-60.729	-43.806	74.880	0.686
16		5.540	570.997	2.986	-1.929	234.067	-151.208	278.660	-3.068	-2.026	-240.524	-158.783	288.208	0.613

All of the BSE, tilt and Strehl ratio is plotted as figure 3.18 and Strehl is plotted as figure 3.19. Error bar at each graph means 95% confidence interval on the mean. Standard deviation is acquired for each set of altitude population mean is estimated. Average value and maximum value for each altitude is presented as table 3.5.

There seems no relation between maximum value and altitude. For the average value, BSE and tilt increase when altitude is decreased, and Strehl ratio is increased while altitude is increased. Since air is sparser at lower altitude effect of aero-optics seems to be less. In hypersonic flow field, shock wave induce BSE of 80 ~ 150 μrad and it means that when target is 10 km far away, 0.8 m~ 1.5 m position error will occur. Overall light system performance, which is Strehl ratio, will also decrease for 0.8.

Table 3.5 Average and maximum value of aero-optical characteristics.

Condition / Altitude	BSE [μrad]		Tilt [μrad]		Strehl Ratio
	Average	Maximum	Average	Maximum	
29.1 km	157.487	278.660	2.104	3.677	0.647
32.3 km	98.139	130.927	1.296	1.810	0.835
38.6 km	84.638	158.764	1.157	2.124	0.797

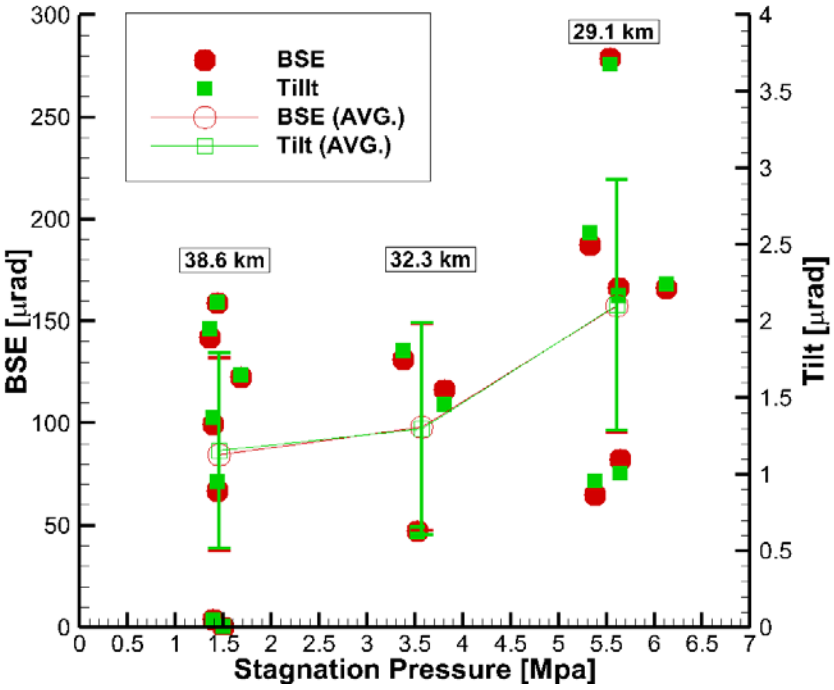

Figure 3.18 BSE, tilt depending on stagnation pressure.

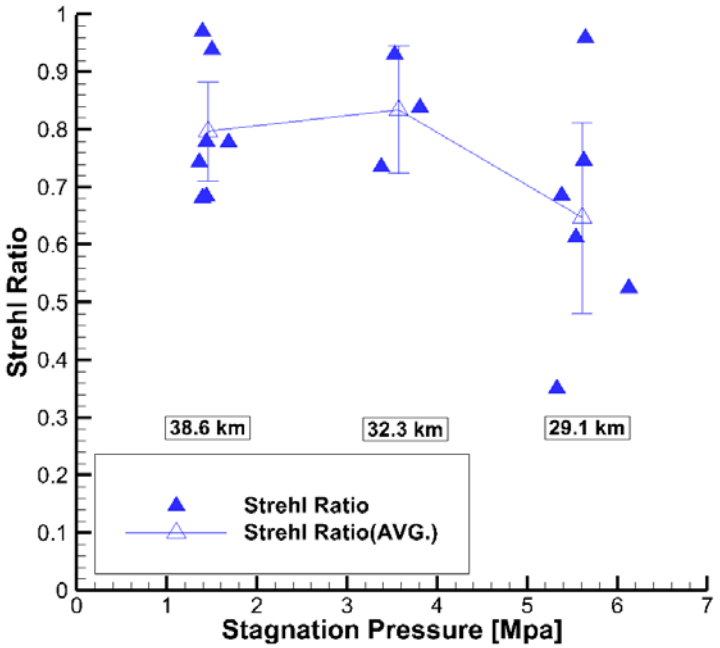

Figure 3.19 Strehl ratio depending on stagnation pressure.

4. Conclusion

Experiment is conducted to study hypersonic flow field characteristics. Shock tunnel is used to demonstrate hypersonic flow field on ground. Shock tunnel performance is validated through driven tube pressure measurement and test time measurement at test section. Measured shock speed is slightly different with theory calculated shock speed due to error during measurement. Most reliable value is pressure at state 2 in the driven tube and stagnation pressure is calculated using this value throughout the thesis. Test time is long enough for aero-optics experiment. Conical nozzle and contoured nozzle is used to generate Mach 7 flow. Wedge model with pitot tube is used to measure Mach and pressure loss. Pitot rake is used to measure flow distribution by radial direction. Conical nozzle has Mach 6.8 flow at the exit and effective diameter is 120 mm. Contoured nozzle has Mach 7 flow at the exit and effective diameter is 144 mm.

Aero-optics experiment is held in static flow and hypersonic flow. Static flow experiment is held to study Shack-Hartmann sensor characteristics. Wedged window validated Shack-Hartmann sensor by comparing measurement result and calculated refractive angle. Hot wire result showed increase of optical aberration as heat increased. Aero-optics experiment model is designed and installed inside shock tunnel test section to study shock wave effect on aero-optical characteristics. 10° wedge model is used to generate shock wave. 635 nm diode laser, which is the object of Shack-Hartmann sensor, is directed perpendicular to wedge model surface. Aero-optical experiment is held for conical and contoured nozazle. In hypersonic flow field, shock wave induce BSE of 80 ~ 150 μrad and it means that when target is 10 km far away, 0.8 m~ 1.5 m position error will occur. Overall light system performance, which is Strehl ratio, will also decrease for 0.8.

Bibliography

[1] E. J. Jumper, and E. J. Fitzgerald, “Recent advances in aero-optics,” *Progress in Aerospace Sciences*, vol. 37, no. 3, pp. 299-339, 4//, 2001.

[2] M. S. Holden, “Calibration and Validation Studies in the LENS Facility,” *Defense Technical Information Center*, 1994.

[3] M. S. Holden, “A Preliminary Study Associated with the Experimental Measurement of the Aero-Optic Characteristics of Hypersonic Configurations,” *CALSPAN-UB RESEARCH CENTER*, vol. ADA-A253 792, 1992.

[4] J. E. A. John, and T. G. Keith, *Gas Dynamics*: Pearson Prentice Hall, 2006.

[5] L. Hyoung-Jin, L. Bok-Jik, K. Sei-Hwan, and J. In-Seuck, “Design/Construction and Performance Test of Hypersonic Shock Tunnel : Part Ⅱ: Construction and Performance Test of Hypersonic Shock Tunnel,” *Journal of The Korean Society for Aeronautical and Space Sciences*, vol. 36, no. 4, pp. 328-336, 4, 2008.

[6] S. Y. Kim, S. D. Kim, I.-S. Jeung, J. K. Lee, and J. Y. Choi, “Boundary Layer Correction of Hypersonic Wind-tunnel Nozzle Designed by the Methods of Characteristics,” *Journal of The Korean Society for Aeronautical and Space Sciences*, vol. 42, no. 12, pp. 1028-1036, 2014.

초 록

극초음속 유동 내 충격파에 의한 공기광학 특성

비행체 주위의 극초음속 유동장은 복잡하여 많은 문제를 야기한다. 특히 광학 체계를 탑재한 비행체 주위의 극초음속 유동장은 공기광학 현상을 유발한다. 공기광학은 비행체 주위에서 유동과 전자기파의 상호작용을 연구하는 분야이다. 비행체 주위의 난류, 충격파 및 경계층은 전자기파의 굴절률을 변화시키고 통과하던 전자기파를 왜곡시킨다. 공기광학 현상은 광학 품질은 저하하여 비행체에 탑재한 광학 체계의 정확도를 제한한다. 따라서 유동장 특성과 광학 특성 사이의 연관성을 찾기 위한 연구가 수행되어 왔다. 이에 따라 공기광학 특성을 분석하고 계측할 수 있는 다양한 센서가 개발되어 왔다. 최근에 샥-하트만(Shack-Hartmann) 센서가 개발되었고 다른 장치와 비교하여 성능이 검증되었다.

본 논문에서는 충격파 풍동(Shock tunnel)을 이용하여 극초음속 유동장을 모사하고 공기광학 실험을 수행한다. 충격파 풍동의 driven tube 에서 충격파 형성에 의한 압력 분포를 분석하고 시험부에서의 시험 시간을 계측하여 성능을 검증하였다. 원뿔형 노즐(Conical nozzle)과 컨투어노즐(Contoured nozzle)을 충격파 풍동에 장착하여 마하 7 유동을 발생시켰다. 노즐의 유동 특성을 분석하기 위해 피토레이크를 이용하여 정체 압력을 측정하고 쉐도우그래프(Shadowgraph) 또는 쉴리렌(Schlieren) 기법을 이용하여 유동을 가시화 하였다. 원뿔형 노즐의 출구 유동은 마하 6.8 이며 63% 정도의 정체 압력 손실이 발생한다. 컨투어 노즐의 경우 정체 압력 손실이 거의 발생하지 않으며 출구 유동은 마하 6.9 이다.

충격파 풍동의 성능 및 노즐의 성능 검증이 이루어진 후 샥-하트만 센서를 이용하여 공기광학 특성을 분석하였다. 샥-하트만 센서의 특성을 연

구하고 극초음속 유동에서의 공기광학 특성을 분석하였다. 광학 테이블 위에서의 실험을 통하여 샥-하트만 센서의 성능을 분석하고 검증하였다. 한 쪽 면이 경사진 유리(Wedged window)와 핫와이어(Hot wire)를 사용하여 밀도 교란을 부여하였다. 경사진 유리를 통과한 레이저는 굴절의 법칙을 통해 계산한 각도를 따라서 굴절하였다. 핫와이어 실험에서는 주입한 전력의 크기가 증가할수록 광학 수차가 증가하는 것을 관찰하였다. 극초음속 유동에서 충격파에 의해 발생하는 공기광학 수차를 계측하였다. 충격파 풍동 시험부에 쐐기 실험 모델을 설치하여 충격파를 발생시키고 샥-하트만 센서로 광학 수차를 계측였다. 샥-하트만 센서는 파면과 세기를 계측하며, 이 들 값을 PSF(Point spread function)로 변환한다. PSF 로부터 BSE, Strehl 비와 같은 공기광학 특성을 계산하였다. 실험 결과 정체 압력이 증가할수록 평균 BSE 및 평균 기울기가 증가하는 특성을 보였다. 충격파에 의한 평균 BSE 는 80 ~ 160 μrad 수준이었고 Strehl 비는 0.65 ~ 0.835 수준이었다. 극초음속 유동장 내의 충격파에 의해 BSE 및 기울기는 증가하고 Strehl 비는 감소한다.

주요어 : **극초음속 유동**, **충격파 풍동**, **공기광학**, **샥-하트만 센서**,

학 번 : 2013-20694